C.P. No. 1235

C.P. No. 1235

PROCUREMENT EXECUTIVE, MINISTRY OF DEFENCE

AERONAUTICAL RESEARCH COUNCIL

CURRENT PAPERS

Some Aerodynamic Considerations of the Flight Characteristics of Towing Systems Using Long Towlines at High Speeds

by

D. Pierce and L. J. Beecham

Aerodynamics Dept., R.A.E, Farnborough

LONDON: HER MAJESTY'S STATIONERY OFFICE

1972

PRICE 95 *p* NET

Current Paper No.1235

CORRECTION

Page 16, line 13 should read:

"The error is seen to be less than 0.1%"

Aeronautical Research Council
London: Her Majesty's Stationery Office

March 1973

CP No.1235*
July 1968

SOME AERODYNAMIC CONSIDERATIONS OF THE FLIGHT CHARACTERISTICS OF TOWING SYSTEMS USING LONG TOWLINES AT HIGH SPEEDS

by

D. Pierce
L. J. Beecham

Aerodynamics Department, RAE Farnborough

SUMMARY

This Paper describes wind-tunnel experiments at supersonic speeds on the characteristics of the three-dimensional growth of turbulent boundary layers on long axi-symmetrically placed wires.

The results have led to the development of a method of calculating the tension and drag distribution along, and the shape of, long towlines as used in aircraft target towing systems.

* Replaces RAE Technical Memorandum Aero 1082 - ARC 34018

CONTENTS

1 INTRODUCTION

The work described in this Paper was undertaken initially in support of a programme involving the towing of targets at supersonic speeds on long towlines. In particular, reliable target and line drag estimates were required to establish the thrust margin of the towing aircraft.

However, it rapidly became clear that the characteristics even of subsonic towlines were not properly understood. Stevens[2] quotes large discrepancies between estimated and measured line drags, and the design of towlines has therefore tended in the past to be based on empirical skin friction coefficients obtained from practice. The present work therefore has included an examination of the subsonic characteristics in an attempt to put the design on to a more rational basis, although no further subsonic wind-tunnel tests have been undertaken. In the absence of suitable supersonic data however, some tunnel tests were carried out to determine the skin friction at supersonic speeds, and, by flow measurements, to obtain an insight into the mechanics of the development of a highly three-dimensional boundary layer.

The latter, backed up by the results of other work[8], has led to the abandonment of the concept of a continuous, single boundary layer development along the line, with the large thickness and low drag that this could imply. The result has produced an estimation method for skin friction in fair agreement with experiment, and not confined to supersonic speed, nor to air, and this, together with available information on the force component derived from the cross flow velocity, is used to give expressions defining the wire tension and shape in a tractable form. Comparisons with limited subsonic flight data are made which give confidence in the application of the method to the prediction of the flight characteristics of supersonic towing systems.

2 SKIN FRICTION OF LONG WIRES

2.1 Existing theoretical methods

Because of difficulties with regard to the three-dimensional growth, the majority of theoretical work on the skin friction of long wires has been confined to laminar flow calculations. One such treatment of the problem is that developed by Glauert and Lighthill[1]. Stevens[2] using this method computed that, compared with results obtained from flight trials, this theory gave numerical values too low by a factor of forty. In the calculations, the boundary layer had been assumed to grow continuously along the whole length

of the wire and the affect of cross flow on the boundary layer had been ignored. This assumption will be shown later to be a major contributory cause of the large discrepancy between theory and flight experiments; furthermore the flight results will be shown to conform more closely to theory based on a turbulent boundary layer.

With regard to three-dimensional growth of turbulent boundary layers Eckert[6] has developed a simplified treatment for a cylinder in axial flow. The calculation is carried out by means of a momentum theorem with assumptions that the velocity profile (1/7 power law) and an empirical relation specifying the wall shear stress as inversely proportional to the fourth root of the boundary layer thickness (Blasius law) are unaffected by the three-dimensionality.

The assumptions imply, and the calculations given in Eckert's note refer, to conditions where the thickness of the boundary layer, δ, is small compared with the radius of the cylinder. In the experiments described in section 2.2 the boundary layer thickness varied between one and thirty times the wire radius. Although the experimental conditions therefore extend far beyond the range of Eckert's assumptions it will be shown that the results appear to be consistent with his calculations, and that for the range of parameters likely to be attained in practice a form of his equation can be used to provide an adequate approximation for skin friction coefficients.

2.2 Supersonic wind-tunnel measurements

The experiments were made in the No.8 (9 in x 9 in) supersonic wind tunnel at R.A.E. Farnborough, at a Mach number of 2.47.

Five diameters of wire ranging from 0.022 in to 0.250 in were tested so that the effect of the ratio of boundary layer thickness to wire diameter could be studied. The wires were tensioned by turnbuckles between two anchor points, one in the settling chamber upstream of the sonic throat and one well downstream of the working section area. The wires were aligned with the stream direction.

Pitot traverses were made through the boundary layer, using a $\frac{1}{2}$ mm o/d hypodermic tube, and were made in the vertical plane above and below the wire at five longitudinal locations throughout the working section. Narrow circular bands of plastic sleeving were put on the wire 8 in upstream of the first traverse location to initiate artificial boundary layer transition to the turbulent state if natural transition had not already occurred.

The position of the probe relative to the wire was determined to an accuracy of 0.002 in by using a microscope viewing the probe through the glass walls of the tunnel. The total head in the boundary layer was measured on a self-balancing capsule manometer to an accuracy of ±0.01 in Hg. The free stream Mach number and static pressure were obtained by relating the free stream total head in the working section to that in the settling chamber.

It should be noted that the outside diameter of the boundary layer probe is approximately equal to that of the smallest diameter wire tested so that for the cases of the smaller wires the total head recorded is the mean pressure over a relatively large area.

At several locations appreciable differences occurred between the boundary layer profiles above and below the wire. These were believed to be a consequence of slight variations in flow direction along the axis of the tunnel nozzle causing the boundary layer to move off-centre relative to the wire.

2.3 Results

2.3.1 Measurement of momentum and velocity profiles

The velocity profiles, and momentum and displacement areas were determined for each of the wires at stations 3 in apart throughout the working section. Although, as explained, differences occur between the upper and lower readings at several stations, the average of the two results show fairly consistent trends with both the wire diameter and probe position as can be seen from Table 1. Nevertheless, individual results are not accurate enough to estimate local skin friction coefficients. Analysis has therefore been based on the mean skin friction between a virtual origin and the appropriate point.

It can be observed that the mean skin friction coefficient and the exponent, n, of the velocity profile given by $v/V = (y/\delta)^{1/n}$, are strongly influenced by the ratio of the length to diameter of the wire. Fig.1 shows how the exponent n rises with ℓ/d from the two-dimensional flat plate value of roughly 6. Values of n are recorded which are much higher than those obtained by Nikuradse[3] for velocity distributions within smooth pipes. Whereas Nikuradse for internal flow shows the exponent to depend only on a Reynolds number based on tube diameter, we see from Table 1 that this is no longer so for the external flow, since at constant R_e we have values of n ranging from 7 to 18 depending on ℓ/d.

To obtain ℓ/d and to calculate the mean skin friction coefficient, C_F, from the momentum area, it was first necessary to determine the virtual origin of the boundary layer. Because of the variation of n, it was not possible to determine this directly. However we assume that, due to the three-dimensional growth, the boundary layer thickness will be no greater than that developed on a flat plate in the same length. From the boundary layer thickness at the first traverse position and the flat plate equation $\delta = \frac{0.37\,\ell}{R_e^{1/5}}$ we can therefore determine the minimum distance of the virtual origin from the traverse position.

The total momentum decrement at any station may be equated to the total drag developed between the virtual origin and that point, thus by extrapolating back the momentum area results we can again deduce a virtual origin. Since the local skin friction, and hence the slope of the actual momentum area curve, reduces with increasing length, a linear extrapolation of the results will give a maximum distance for the virtual origin from the first traverse position. The distance between the maximum and minimum positions should reduce as the value of $n \to 7$. The mean of these positions gives locations for the virtual origin estimated to be within 3 in of the true position. Owing to scatter, extrapolation of the momentum results for the 0.25 in diameter wire is difficult. Since for these results n is close to 7, values of ℓ equal to ℓ_{min} + 2 in have been used.

Using the above method of estimating the position of the virtual origin for each of the wires, the mean skin friction coefficients, Table 1, have been calculated. The coefficients, based on wetted area, are shown in Fig.2 plotted against Reynolds number. Also shown is a curve representing the value calculated using Schlichting's[4] flat plate equation modified by a compressibility factor given by Hoerner[5]. It can be seen that the results for the 0.25 in diameter wire lie close to this line as might be expected since the values of n for these results are only slightly greater than that for the flat plate, but that there is increasing discrepancy as the thickness increases.

Using a simplified treatment of the turbulent boundary layer along a cylinder, Eckert[6] has deduced an expression for the mean skin friction coefficient, for cases where the boundary layer thickness is less than the radius of the wire.

This expression can be re-arranged in the form:-

$$C_F = C_{F_P}\left[1 + f\left(\frac{\delta}{d}\right)\right] \qquad (1)$$

where C_{F_P} is the skin friction coefficient for an infinite flat plate.

Since Eckert has assumed that the velocity profile (1/7 power law) is unaffected by the curvature we may substitute $\frac{0.37\,\ell}{R_e^{1/5}}$ for δ giving

$$C_F = C_{F_P}\left(1 + \frac{A'\,\ell/d}{R_e^{1/5}}\right) \qquad (2)$$

where ℓ and R_e are based on the length from the virtual origin, and A' is a factor which reduces from 0.025 as $\frac{\ell/d}{R_e^{1/5}}$ increases from zero.

For all diameter wires except the largest the experimental results have shown that the value of n greatly exceeds the assumed value of 7. Again, the boundary layer may no longer depend on $R_e^{1/5}$ and in any case its thickness exceeds the radius of the wire. The use of the Eckert's value of A' may therefore not be justified; on the other hand Fig.2 shows that C_F does depend appreciably on wire diameter and slightly on R_e, as equation (2) qualitatively predicts, and it would seem possible that by choosing some suitable value of A' the results may be shown to conform to this equation. The mean value of A' for the range of $\frac{\ell/d}{R_e^{1/5}}$ covered during the present experiments is taken to be 0.017.

Fig.3 shows the C_F results of Fig.2 divided by $\left(1 + \frac{0.017\,\ell/d}{R_e^{1/5}}\right)$ to give $\bar{C}_F$. The results collapse surprisingly well considering the possible errors and lie reasonably close to the Schlichting flat plate curve with the compressibility modification.

From this evidence it would appear that equation (2) provides a convenient and reasonably accurate way of estimating skin friction in a turbulent three-dimensional boundary layer despite the fact that integration of the momentum loss throughout the boundary layer is not always a satisfactory method of deducing skin friction coefficients from experimental data.

In Ref.7, Hughes describes tests at the N.P.L. on long cylinders submerged in water. During these tests the drag of the cylinders at different

velocities was measured directly by a very sensitive balance system. The ratio of length to diameter for these tests were 340, 673 and 1004 and are therefore within the range covered by the present series of tests of 106 to 1250. Since the drag was measured directly the results should be more reliable than those obtained by boundary layer measurements (section 2.2). The results are shown in Fig.4. Using equation (2) with A' again equal to 0.017 we see (Fig.5) that expression in terms of the parameter $\bar{C}_F$ effectively collapses these results also to the Schlichting two-dimensional curve. Fig.5 indicates that if necessary an even better collapse could be obtained using a larger value of A' for the $\ell/d = 340$ results and a smaller value for the $\ell/d = 1004$ results. This is in accord with the reduction of A' with the increase of $\frac{\ell/d}{R_e^{1/5}}$ for the Eckert equation.

These results have been obtained by direct variation of the velocity and cover a far wider range of Reynolds number than the wind-tunnel results described in this Paper.

We see therefore that the skin friction deduced from experiments at low velocity in water and at supersonic speeds in air, can be represented by the same expression, viz.

$$C_F = \frac{0.455\ (\log_{10} R_e)^{-2.58}}{(1 + 0.15\ M^2)^{0.58}} \left(1 + \frac{0.017\ \ell/d}{R_e^{1/5}}\right) \quad . \qquad (3)$$

2.3.2 Effect of length

If we examine the values of C_F computed from equation (3) for various lengths of the same diameter wire we find for a typical example (Fig.6), that for short lengths the skin friction falls according to the Schlichting equation. Gradually as the length increases the three-dimensional part of equation (3) takes effect and the skin friction coefficient levels off and then begins to rise. For a length 4000 times its diameter the mean skin friction coefficient is the same as if it were 10 times its diameter. At its lowest value between these lengths the value of C_F has fallen by 36%.

We see therefore that provided that the length over which the boundary layer grows is unlikely to exceed 4000 times the wire diameter in this case, we can, for a rough approximation of friction drag assume a fixed value of C_F which in this particular example is unlikely to have a local error at any position of more than 18%. Although this error is not negligible it

should be remembered that by assuming the theory of Glauert and Lighthill numerical values too low by a factor of 40 were obtained. It will be shown later that, because of the curvature of the wire, parts of the wire where the assumed drag is too small will be offset by other regions in which the assumed drag is too great. This suggests that along a given towline it might be justifiable to regard C_F as effectively constant, an assumption which greatly simplifies the estimation of the curvature of the wire and of the cross flow drag as described later. This is considered further in section 2.4.

The theory of Glauert and Lighthill can be used to determine C_F for various lengths of a laminar boundary layer in a similar form to Fig.6. Calculations for the same typical conditions of Fig.6 are shown in Fig.7. We see that the curve again represents a flat plate skin friction coefficient plus a three-dimensional effect. The slope of the curve is much steeper than that for the turbulent boundary layer and an assumption of a constant C_F would be far less justifiable.

2.3.3 Effect of incidence

Up to the present we have considered only the boundary layer growth on a wire trailing in the stream direction.

Thompson and Morrison[8], investigating the asymmetric shedding of vortices from slender bodies at large angles of yaw, have obtained Schlieren pictures of the periodic shedding of the boundary layer. Similar results have been obtained during the present series of tests when a $\frac{1}{4}$ in diameter rod was placed at incidence. Typical spark and continuous source Schlieren pictures at M = 1.5 are shown in Fig.8.

The periodic shedding observed in these pictures is confirmed by the oil flow pattern, Fig.9, formed on the downstream surface of the rod. The vortices grow symmetrically from the nose until due to some disturbance one sheds. Thereafter vortices grow and are shed alternately from either side.

The report[8] explains how the shedding on a cylinder at incidence can be related to the frequency with which the vortices forming a Kármán vortex street would be shed from the cylinder if it were placed normal to the stream. The relationship is given by

$$s = \frac{f\,d}{V_\infty \sin \alpha}$$

where s = Strouhal number

f = frequency of shedding (from one side only)

d = cylinder diameter

V_∞ = free stream velocity

α = incidence of the cylinder.

Now $\frac{1}{f}$ is the time interval between the instants at which successive vortices are shed from the same side, and is also the time taken for the flow component with velocity $V_o \cos \alpha$ to travel a distance $\bar{\ell}$. In this instance $\bar{\ell}$ represents the length over which the boundary layer grows before it sheds.

Thus
$$\frac{1}{f} = \frac{\bar{\ell}}{V_\infty \cos \alpha}$$

and
$$\frac{\bar{\ell}}{d} = \frac{\cot \alpha}{s} \quad . \qquad (4)$$

The effect on skin friction coefficient, of wire incidence is therefore that the development of the boundary layer should no longer be considered as continuous, but that the coefficient should be determined for the shedding length $\bar{\ell}$. Since, as shown in Figs.6 and 7, C_F falls as $\bar{\ell}$ increases we see that the greater the incidence, the shorter the shedding length and the higher the skin friction coefficient.

As the shedding length reduces it is conceivable that the boundary layer might remain laminar for a substantial part of its length. To examine the likelihood of this occurring in practice we can compare the calculated skin friction coefficients for a laminar and a turbulent boundary layer with those deduced from flight trials.

Taking values of towline incidence as quoted by Stevens[2] and assuming values of $s = 0.20$ for a laminar boundary layer and $s = 0.30$ for a turbulent one we are able to estimate the appropriate shedding lengths and hence skin friction coefficients. The results are as follows:-

		V_∞ (ias)	175 kt	300 kt
Measured	C_F	(flight trials)	0.0059	0.0050 from Ref.2
Estimated	C_F	(turbulent boundary layer)	0.0050	0.0045 from equation (3)
Estimated	C_F	(laminar boundary layer)	0.0016	0.0011 from Ref.1

In the following sections we therefore assume that the boundary layer is turbulent and that equation (3), with shedding length $\bar{\ell}$ replacing the total

wire length, provides a satisfactory approximation of the skin friction coefficient.

2.4 Suggested estimation method

Equation (3) gives an expression for the skin friction coefficient for a long wire, including compressibility and three-dimensional effects, in terms of $R_e(\ell)$, ℓ/d and M, where from 2.3.3 we interpret ℓ as the length of wire for which the boundary layer remains locally attached. This length is variable along the wire depending as has been shown, on the local incidence, and hence both $R_e(\ell)$ and ℓ/d are functions of incidence. Equation (3) may therefore be more conveniently expressed in terms of wire diameter, incidence and flight Mach number.

Thus, from equation (4),

$$R_e \left(\equiv \frac{V\ell}{\nu} \right) = Md \cot \alpha \frac{a}{\nu s}$$

$$= Md^* \cot \alpha \frac{a_o}{\nu_o s}$$

where $d^* \left(\equiv d \cdot \frac{a}{\nu} \frac{\nu_o}{a_o} \right)$ is the equivalent wire diameter at ground level. The effect of altitude is to reduce the effective diameter (Fig.12) in the determination of R_e. It should be noted that the actual diameter, d, is retained in the definition of the force coefficients.

Assuming a Strouhal number of 0.3 appropriate to a turbulent boundary layer,

$$R_e = Md^* \cot \alpha \times 2.38 \times 10^7 \qquad (d^* \text{ in ft})$$

and

$$C_F = C_F(M, d^*, \cot \alpha) = \frac{0.455 \, (\log R_e)^{-2.58}}{(1 + 0.15 M^2)^{0.58}} \left(1 + \frac{0.017}{0.3} \cdot \frac{\cot \alpha}{R_e^{1/5}} \right) \cdot \quad \ldots\ldots (5)$$

Skeleton plots of C_F for a subsonic vs a supersonic flight speed over representative wire diameters and incidences are shown in Fig.13. From these it can be seen that although the incidence may vary considerably along a wire

in particular conditions, the local skin friction varies more slowly, and for the purpose of estimating wire shape and tension a mean value might well suffice. In the computations made in section 5.2 a mean incidence of 5° has been used for the purpose of estimating the skin friction coefficient from equation (5) as an average of the asymptotic incidences of the flight data considered therein. A refinement is suggested in section 6.

3 CROSS FLOW FORCE

It is well known that the force normal to a long, inclined body at supersonic speeds is not linear with the incidence angle. Rather it consists of two portions, viz. that given by a potential flow, giving a force linear with incidence, and dependent only on the way in which the cross section area varies along the length, and additionally a viscous force due to flow separation on the lee of the body. At any particular Mach number this latter force contribution is proportional to the cross flow kinematic pressure so that it can be represented by $C_D \cdot \frac{\rho V^2}{2} \sin^2 \alpha \cdot S$ where V is the free stream velocity and S is the maximum body area normal to the cross flow. This has been found to predict remarkably well the normal force on bodies of moderate fineness ratio at supersonic speeds[9], and, since the cross flow Mach number, M_c, as opposed to the free stream Mach number, is usually well subsonic, a commonly used value of C_D for supersonic flight is 1.2, factored where necessary for the effect of the finite fineness ratio[9] (Fig.10). For the present purpose the wire constitutes effectively an infinitely long body for which the potential flow term is negligible. We would expect the cross flow force to be $D\ell \sin^2 \alpha$, where $D = q\, C_D\, d$ and with C_D approximately constant at about 1.2. Fig.11 is reproduced from Ref.9 and shows that the drag of circular cylinders normal to a low speed airstream for a Reynolds number based on diameter between 10^4 and 10^5 is appropriate to a C_D of about 1.2, and between 10^3 and 10^4 is generally nearer unity. Below 10^3 C_D increases again. The good agreement obtained at supersonic speed with a C_D of 1.2 has been with inclined cylinders for which the typical cross flow Reynolds numbers have been between 10^4 and 10^5. For a small gauge wire towline the cross flow R_e would be about two orders smaller so that C_D might be expected therefore to be somewhat below 1.2. The comparisons with subsonic flight data made in this Paper in section 5.2 do not show conclusively whether the preferred value should be 1.2 or nearer 1.0. Further flight measurements are needed.

4 TOWLINE SHAPE AND TENSION

4.1 Equations

The equations derived in this section are those applicable to the forces on a wire being towed by an aircraft in straight and level flight, and as such are confined to the vertical plane.

The forces on an element are shown in Fig.14, resolved along and normal to the wire.

(1) Incremental tension, taking account of the curvature of the element, is

$$\begin{bmatrix}\text{Tensile force along}\\ \text{Tensile force normal}\end{bmatrix} = \begin{bmatrix}1 & -\delta\alpha\\ \delta\alpha & 1\end{bmatrix}\begin{bmatrix}T+\delta T\\ 0\end{bmatrix} - \begin{bmatrix}T\\ 0\end{bmatrix} = \begin{bmatrix}\delta T\\ T\delta\alpha\end{bmatrix} .$$

(2) Aerodynamic force

$$\begin{bmatrix}\text{Friction force along}\\ \text{Cross flow force normal}\end{bmatrix} = \begin{bmatrix}-F\cos^2\alpha\,.\,\delta\ell\\ \operatorname{sgn}\alpha\,.\,D\sin^2\alpha\,.\,\delta\ell\end{bmatrix}$$

where F and D are regarded as constant throughout the wire length (sections 2.4 and 3), and

$$\operatorname{sgn}\alpha = \alpha \div |\alpha| .$$

(3) Weight

$$\begin{bmatrix}\text{Component along}\\ \text{Component normal}\end{bmatrix} = \begin{bmatrix}-\omega\sin\alpha\,.\,\delta\ell\\ -\omega\cos\alpha\,.\,\delta\ell\end{bmatrix}$$

where ω = weight of wire per unit length.

Combining these and equating for equilibrium we have:-

$$\text{Force along wire :}\quad \frac{dT}{d\ell} = \omega\sin\alpha + F\cos^2\alpha \qquad (6)$$

$$\text{Force normal to wire :}\quad \frac{Td\alpha}{d\ell} = \omega\cos\alpha - \operatorname{sgn}\alpha\, D\sin^2\alpha . \qquad (7)$$

If we divide (6) by (7) we eliminate the length parameter, so that

$$\frac{1}{T} \cdot \frac{dT}{d\alpha} = \frac{\omega \sin\alpha + F \cos^2\alpha}{\omega \cos\alpha - \operatorname{sgn}\alpha \cdot D \sin^2\alpha}$$

from which

$$\log \frac{T}{T_o} = \int_{\alpha_o}^{\alpha} \frac{\omega \sin\alpha + F \cos^2\alpha}{\omega \cos\alpha - \operatorname{sgn}\alpha \cdot D \sin^2\alpha} \, d\alpha \qquad (8)$$

where suffix o denotes conditions at the target.

$\left(\text{N.B.} \quad \tan\alpha_o = \frac{\text{weight - lift}}{\text{drag}} \text{ of target.}\right)$

Hence, from (6) and (8),

$$\ell = \int_{\alpha=\alpha_o}^{\alpha=\alpha} \frac{dT(\alpha)}{\omega \sin\alpha + F \cos^2\alpha} \; . \qquad (9)$$

4.2 Method of solution

It will be seen from equations (8) and (9) that the variables have been separated, and that the solutions for $\ell = \ell(\alpha)$ and $T = T(\alpha)$ can be obtained in principle by direct integration. For convenience we write the r.h.s. of equation (8) as $\left[\frac{F}{\omega} I_1 + \frac{F}{\omega} I_2 + I_3\right]_{\alpha_o}^{\alpha}$

where $I_1 = \int \frac{d\alpha}{\cos\alpha - \operatorname{sgn}\alpha \frac{D}{\omega} \cdot \sin^2\alpha}$

$$I_2 = -\int \frac{\sin^2\alpha \, d\alpha}{\cos\alpha - \operatorname{sgn}\alpha \frac{D}{\omega} \cdot \sin^2\alpha}$$

$$I_3 = \int \frac{\sin\alpha}{\cos\alpha - \operatorname{sgn}\alpha \frac{D}{\omega} \cdot \sin^2\alpha} \; .$$

Integrating, and omitting the integration constant,

$$I_1 = \frac{\sin \alpha_\infty}{(1 + \cos^2 \alpha_\infty)} \left\{ \log \left| \frac{(1 + \text{sgn } \alpha \cos \alpha_\infty) \tan \frac{\alpha}{2} + \sin \alpha_\infty}{(1 + \text{sgn } \alpha \cos \alpha_\infty) \tan \frac{\alpha}{2} - \sin \alpha_\infty} \right| \right.$$

$$\left. - \text{sgn } \alpha \, 2 \cos \alpha_\infty \tan^{-1} \left| \left(\frac{1 - \text{sgn } \alpha \cos \alpha_\infty}{\sin \alpha_\infty} \right) \tan \frac{\alpha}{2} \right| \right\}$$

.... (10)

where α_∞ is the incidence such that $\frac{D}{\omega} = \frac{\cos \alpha_\infty}{\sin^2 \alpha_\infty}$. This corresponds to the asymptotic incidence of the wire, at the towing aircraft, for which $\frac{d\alpha}{d\ell}$ is zero (equation (7)).

It may be shown that

$$I_2 \doteqdot - \sin^2 \alpha_\infty [I_1 - \alpha]$$

and

$$I_3 = \frac{\sin^2 \alpha_\infty}{1 + \cos^2 \alpha_\infty} \log \left| \frac{\cos \alpha - \cos \alpha_\infty}{\cos \alpha + \sec \alpha_\infty} \right| \quad . \qquad (11)$$

Since at high speeds F is large in comparison with ω it follows that the contributions from I_2 and I_3 are of the order of $\sin^2 \alpha_\infty I_1$, and hence, since $\sin^2 \alpha_\infty$ is small at high speeds, it is proposed to neglect all except I_1,

i.e. $$\int \frac{\omega \sin \alpha + F \cos^2 \alpha}{\omega \cos \alpha - \text{sgn } \alpha \, D \sin^2 \alpha} d\alpha \doteqdot \frac{F}{\omega} I_1 \quad . \qquad (12)$$

However, the expression for I in equation (10) does not lend itself to the inversion necessary to give α as $\alpha(\ell)$. It is possible to make it more tractable, however, by a slight approximation before integration, viz. by approximating for $\omega \cos \alpha$ in denominator by $\omega \left(1 - \frac{\sin^2 \alpha}{2}\right)$. With this modification, but with the adoption of the correct rather than the approximate asymptotic incidence, it transpires that

$$I_1 \doteqdot \frac{\tan \alpha_\infty}{2} \log \left| \frac{\tan \alpha + \tan \alpha_\infty}{\tan \alpha - \tan \alpha_\infty} \right| \qquad \text{for } \alpha \text{ +ve} \qquad (13)$$

and $$\doteqdot - \sin \alpha_\infty \tan^{-1} \left[\frac{\tan \alpha}{\sin \alpha_\infty} \right] \qquad \text{for } \alpha \text{ -ve} \quad . \qquad (14)$$

For the incidence to be negative requires that there shall be lift on the target in excess of its weight, a case which is not considered further in the present Paper. The suitability of the approximation (equation (14)) for negative incidence has therefore not been examined. Equation (13) for positive incidence does include the case of the very light, or partially lifting, target for which $\alpha_o \leqslant \alpha \leqslant \alpha_\infty$. In this condition the towline curvature is reversed.

The justification for the approximation of equation (13) is contained in Fig.15. Equations (10) and (13) were found to give values which are indistinguishable on direct presentation. In Fig.15 the percentage error is shown for a range of maximum and asymptotic incidences up to 45° and 20° respectively to include very heavy targets and tow wires at supersonic speeds. The error is seen to be less than 1%.

Substituting for equation (13) in equation (8) we have

$$\left(\frac{T}{T_o}\right)^{\frac{2D}{F}\sin\alpha_\infty} \doteq \frac{\tan\alpha + \tan\alpha_\infty}{\tan\alpha - \tan\alpha_\infty} \cdot \frac{\tan\alpha_o - \tan\alpha_\infty}{\tan\alpha_o + \tan\alpha_\infty} \qquad (15)$$

or, rearranging,

$$\frac{\tan\alpha}{\tan\alpha_\infty} = \frac{2r + (1 + r)\,\varepsilon}{2 + (1 + r)\,\varepsilon} \qquad (16)$$

where $r = \dfrac{\tan\alpha_o}{\tan\alpha_\infty}$

and

$$\varepsilon = \left(\frac{T}{T_o}\right)^{\frac{2D}{F}\sin\alpha_\infty} - 1 \quad . \qquad (17)$$

The neglect of I_2 and I_3 in comparison with I_1 is tantamount to regarding the numerator of the integrand of equation (8) as constant ($= F$); the error thereby introduced [$= \sin\alpha\,(F\sin\alpha - \omega)$] is of a small order and the separate terms to some extent compensatory. This approximation enables equation (6) to be integrated directly to give

$$T = T_o + F\ell \quad . \qquad (18)$$

Equations (16) and (18) provide simple and convenient expressions from which to obtain the approximate distribution of incidence and tension along a towline in a closed form.

The component drag terms may then be evaluated as

$$\text{wire cross flow drag} = D \int_0^{\ell} \sin^3 \alpha \, d\ell \tag{19}$$

$$\text{wire friction drag} = F \int_0^{\ell} \cos^3 \alpha \, d\ell \tag{20}$$

and the target depression from the flight path of the towing aircraft as

$$h \equiv \int_0^{\ell} \sin \alpha \, d\ell \quad . \tag{21}$$

4.3 Further approximations

When ℓ is small enough, i.e. sufficiently near the target, it is permissible to expand ε (equation (17)) as

$$\varepsilon \equiv \left(1 + \frac{F\ell}{T_o}\right)^{\frac{2D}{F} \sin \alpha_\infty} - 1$$

$$\doteq \frac{2D}{T_o} \ell \sin \alpha_\infty \tag{22}$$

so that

$$\tan \alpha \doteq \frac{\tan \alpha_o + \ell C \tan \alpha_\infty}{1 + \ell C} \tag{23}$$

where C is constant $= (\tan \alpha_o + \tan \alpha_\infty) \frac{D}{T_o} \cos \alpha_\infty$.

It will be observed that the friction force, F, does not enter into any of the constant terms on the r.h.s. of equation (23) which indicates that the terminal shape of the wire at the target is defined by its weight and cross flow drag per unit length together with the target forces.

The approximation of equation (22) cannot be justified for other than small values of ℓ. Nevertheless equation (23) tends to the correct limit as $\ell \to \infty$, suggesting that it may be useful even when it cannot be strictly validated.

The target depression, $h = \int_0^{\ell} \sin\alpha \, d\ell$ and the determination of $\sin\alpha$ from $\tan\alpha$ defined by equation (23) is somewhat troublesome for the subsequent integration. If we consider equation (15) it appears that the r.h.s. would have the same characteristics and behaviour at the limits as $\alpha \to \alpha_o$ or α_∞ if the tangents were replaced by sines throughout. It is suggested therefore that for the purposes of determining the target depression and the terminal length of wire that the sine equivalent of equation (23) might be a reasonable approximation viz.

$$\sin\alpha \doteqdot \frac{\sin\alpha_o + R\ell \sin\alpha_\infty}{1 + R\ell} \qquad (24)$$

where $R = (\sin\alpha_o + \sin\alpha_\infty)\frac{D}{T_o}$.

This may be integrated directly with respect to ℓ to give

$$h \doteqdot \ell \sin\alpha_\infty + \frac{\sin\alpha_o - \sin\alpha_\infty}{\sin\alpha_o + \sin\alpha_\infty} \cdot \frac{T_o}{D} \log_e \left[1 + (\sin\alpha_o + \sin\alpha_\infty)\frac{D}{T_o}\ell\right] \quad \ldots\ (25)$$

$$= P\ell + Q \log_e (1 + R\ell)$$

where P, Q and R are constant along the wire.

5 APPLICABILITY OF METHOD

The validity of expressions derived in the preceding section has been examined in two respects, firstly for their acceptability as solutions to the differential equations (6) and (7), and secondly their practicability when compared with flight data. In the latter some difficulty has been experienced due to the paucity of data at supersonic or high subsonic speeds, and also by the omission or non-availability of certain key data in the references consulted.

5.1 Validity of approximations

The justification for the pre-integration simplification of equation (8), leading to the approximate relationships of equations (16) and (18) between local incidence, tension and length, was discussed in section 4.2. As mentioned therein, the target and wire weights need to be rather extreme for

the error to exceed even 0.1% (Fig.15), and this figure is itself very much smaller than the admitted uncertainties, in the skin friction estimation for example. The effect is illustrated in Fig.16 which shows a barely discernible departure over the first 1000 ft between the exact (step-by-step) solution and that given by equation (16) for the specific case of a supersonic (M = 1.6) towline.

On this same figure is shown the result of simplifying further by the assumption of a short towline (section 4.3). The approximation labelled equation (23) begins to deviate noticeably from the exact result for a line length greater than about 150 ft. But, nevertheless, the incidence is everywhere within a degree, which may be adequate for many estimates.

However, the quantity of main interest from the point of view of adequacy of estimation methods is not the incidence so much as the depression of the target below the aircraft. The comparisons between the step-by-step computations and the approximations of equations (16), (21) and (25) are shown for the same supersonic tow case in Fig.17a. From these it is seen that the difference between the iterative solution of the differential equations (equations (6) and (7)) and the numerical integration with length of $\sin \alpha$, where α is given by equation (16), is barely discernible. For a towline length of 1000 ft the difference is about 6 in. in 126 ft; at 5000 ft it is 2 ft 4 in. in 320 ft. It is noticeable that the short line approximation to the target depression given in closed form by equation (25) is in quite good agreement, the error amounting to about 6 ft for a line length of 1000 ft.

Step-by-step solution data were unfortunately not obtained for the flights reported in Refs.10,11,12, so that comparisons in these cases are made only between the results from equation (21), using the incidence variation computed from equation (16), and those given through the suggested relationship of equation (24). This comparison is shown in Figs.17b and 17c for computations related to data from Refs.10 to 12, and suggest that even at low subsonic speeds the simpler expression, equation (25), may adequately define the terminal shape of the wire for, say, about 200 ft, except possibly at the lowest speed for which the wire incidence at the target is very high (about 65°).

In section 4.3, arising from the short line assumptions, it was pointed out that the skin friction force, F, ought to have little influence on the terminal shape of the wire. The computations associated with Fig.17 included a

10% reduction in skin friction to examine its effect on target depression. The results showed a difference of only 1 ft (in 1360 ft) for a towline length of 20000 ft, thus tending to confirm this predicted insensitivity, which may persist beyond the terminal region.

5.2 Comparison with flight data

5.2.1 Skin friction and wire tension

Following from the pre-integration simplification in section 4.2, the force gradient along the wire was shown to be effectively constant so that the tension should be a linear function of the length (equation (18)). Figs.18a and 18b are reproduced from Refs.10 and 12, and these show this linear dependence over a wide range of flight speeds and towline lengths. The slope at each speed should equate to the skin friction force, F, in section 4. The mean values from the flight data of Refs.10 and 11 at 200 kt and 320 kt ias prove to be 10.2 lb/1000 ft and 23.6 lb/1000 ft respectively, compared with the friction drags, estimated from equation (5), of 11.1 and 25.5 lb/1000 ft respectively. The data from Ref.12 are rather less self consistent but generally confirm the tendency for the estimate to be approximately 10% high. This could be adjusted by choosing an effective incidence of less than the 5° arbitrarily adopted in the evaluation of equation (5), (see section 6), and further experimental data are needed to clarify this point.

5.2.2 Wire shape

Determinations of the target depression in flight have been made[10,11,12] using a chase aircraft with its altimeter synchronised with that of the towing aircraft. No details are known of the proximity of the chase aircraft to the target, so the possibility of aerodynamic interference has not been assessed. No comments were offered in Ref.12 on the scatter and discrepancy between results from, as far as is known, identical tests made 2 months apart in 1959 (Figs.20a to 20d).

Data from Boscombe Down trials[10,11] are given in Figs.19a and 19b, and are compared with the estimated target depression offered in this Paper. In both figures, representing the extremes of the speed range of the trials, the agreement is much improved by the adoption of a cross flow force coefficient of 1.0 rather than 1.2. With this modification and except at the maximum line length of 20000 ft the present method predicts satisfactorily the

vertical separation both at the higher speed ($M \div 0.6$) and also at the lower speed where the simplifications might be thought less defensible.

The U.S.A. data from the Air Proving Ground Centre report[12] are shown in Figs.20a to 20d, and, again except at the maximum line length, the flight test data straddle the estimate. However, in this case the cross flow coefficient of 1.2 does provide the better agreement with flight data.

The fact that in both the AAEE and APGC data the target depression with the 20000 ft line falls noticeably below the estimate is curious, particularly since the corresponding rates of change of depression between the 15000 ft and 20000 ft towline lengths implies a local wire incidence less than the asymptotic minimum value, α_∞ (section 4.2). The explanation may lie in the fact that with extremely long towlines and the correspondingly large vertical separations between aircraft and target, the greater air density at the target altitude and over much of the wire may need to be taken into account. Examination of the flight data on Figs.19 and 20 shows that this reduction in the depression gradient is indeed progressive with length as this explanation would require.

It is noticeable from Figs.19 and 20 that apart from towline lengths less than about 1000 - 2000 ft, the estimated variation of target depression with length is, for all practical purposes, linear, and is given by the asymptotic incidence ($\div (\omega/D)^{\frac{1}{2}}$). This suggests that it may be possible to devise simple working rules for estimating the depression for other than short towlines if the intercept of this straight line at $\ell \simeq 0$ can be expressed in terms of the target weight and drag, i.e. in terms of the terminal incidence of the wire. The reader is advised against utilising Fig.20 directly for this purpose inasmuch as the basic data in Ref.12 apply to a target on which a lift force is present, i.e. the effective weight varies with flight speed. For the comparisons in this Paper the data have been further processed to extract this force, and hence to derive the terminal incidence.

6 GENERAL COMMENTS

It has been mentioned in passing that the computations and the further approximations suggest that the skin friction has little influence on the wire shape. Further, the analytical and experimental results agree in showing that the cross flow drag has negligible effect on the wire tension, which varies linearly with towline length by the amount of the accumulated skin friction drag. Fig.21 shows the distribution of the computed drag along the line for

the supersonic tow case as discussed in section 5.1, viz. M = 1.6 at 40000 ft with steel wire 0.050 in diameter, target weight 100 lb. This distribution for the non-lifting target, is typical for high speeds and shows the majority of the cross flow drag on a practicable towline length* to be developed within the terminal 1000 ft.

From equations (19) and (20) it follows that the rate of increase of the friction drag with length exceeds that of the cross flow drag when $\tan \alpha$ falls below $(F/D)^{1/3}$. For the data examined in this Paper this occurs in a narrow band between $12\frac{1}{2}^{\circ}$ and $14\frac{1}{2}^{\circ}$, i.e. fairly close to the target. It has already been remarked that the high curvature is also localised to the terminal length near the target, the incidence rapidly approaching the asymptotic value. This means that on long lines the majority of the skin friction drag is developed at an incidence near to this asymptotic value and suggests that this, rather than the arbitrary mean of 5° used in section 2.4, should be used as a basis for evaluating C_F from equation (5). This may be readily calculated in advance from a knowledge of the wire weight, ω, and the cross flow drag, D per unit length (section 4.2).

Throughout this Paper it has been assumed that the wire weight will be light so that the maximum wire incidence will occur at the target. This may not always be so, particularly when lifting targets are used, and Fig.21 shows the effect on the target depression and drag of the generation of lift on the target. The cross flow drag is negligible, giving a small overall reduction in the line drag. But this would be offset in practice by the drag-due-to-lift on the target which has not been taken into account in this example.

It is perhaps surprising that there are so few published flight data on the characteristics of high speed towed systems. There would appear to be a good case for an instrumented "target", equipped to telemeter its vertical displacement relative to the towing aircraft and also the tension in the towline at the target. This information, together with the tension in the wire at the point of attachment to the aircraft, would provide all the data necessary for a detailed examination of the applicability of the estimation methods suggested herein, and would enable the data from lifting as well as non-lifting targets to be readily utilised.

---

* Since the line must have some weight, its asymptotic incidence cannot be zero and hence there is no theoretical upper limit to the wire cross flow drag. The limitation is the practical one of the yield stress of the material which in this particular example would be reached at about double the length shown in Fig.21. The cross flow drag would increase by only 1.3 lb in this extra length.

7 CONCLUSIONS

7.1 The boundary layer development on a long wire with any incidence is not continuous. Periodic shedding and redevelopment occurs, the decrease in attachment length producing a much larger skin friction force than would be predicted on the assumption of a single continuous boundary layer.

7.2 A modified form of the Schlichting formula for turbulent skin friction on a flat plate allowing for compressibility and three-dimensionality, and with Reynolds number based on the length over which the boundary layer remains attached has been found to give good agreement with experimental results in air and in water. This is given in equation (5).

7.3 The skin friction thus obtained is comparatively insensitive to the local incidence, and, on the premise that it may be regarded as a constant throughout the length of any particular towline, approximate closed expressions have been derived (equations (16) and (18)) for the tension and incidence along the wire. Limited comparisons with flight data suggest that these relations provide a reasonable basis for the estimation of the steady flight characteristics at both high and low speeds.

7.4 Further simplifications (equations (23) and (24)) are suggested for application over the terminal length of line adjacent to the target which give the approximate depression directly in a closed form. No flight data for comparison have been available. These and computations suggest that, particularly at high speeds, the terminal shape may be regarded as insensitive to the skin friction, and the wire tension as independent of the cross flow force.

ACKNOWLEDGEMENT

The authors are indebted to Mrs. G. Edwards for the programming and performance of the computations in this Paper.

Table 1

Wire diameter in	ℓ in	$R_{e_\ell} \times 10^{-6}$	Displacement ≠		Momentum ≠ area in^2	C_F	n ≠	ℓ/d
			Area in^2	Thickness in				
0.022	18.5	4.62	0.0110	0.049	0.00318	0.00505	15.4	841
	21.5	5.37	0.0122	0.052	0.00342	0.00460	15.2	977
	23.5	6.12	0.0138	0.056	0.00415	0.00489	16.2	1113
	23.5	6.12	0.0136	0.056	0.00363	0.00428	17.0	1113
	27.5	6.87	0.0150	0.059	0.00437	0.00459	18.4	1250
0.037	17.8	4.45	0.0160	0.055	0.00447	0.00432	16.9	481
	20.8	5.20	0.0185	0.061	0.00523	0.00432	11.7	562
	23.8	5.95	0.0183	0.060	0.00530	0.00383	13.8	644
	23.8	5.95	0.0186	0.061	0.00510	0.00368	13.3	644
	26.8	6.70	0.0208	0.066	0.00587	0.00376	15.1	724
	29.8	7.45	0.0235	0.070	0.00644	0.00371	16.0	805
	29.8	7.45	0.0249	0.073	0.00717	0.00413	15.1	805
0.064	18.4	4.60	0.0257	0.064	0.00663	0.00359	11.7	288
	21.4	5.35	0.0290	0.069	0.00769	0.00357	11.0	334
	24.4	6.10	0.0290	0.069	0.00781	0.00318	11.2	381
	27.4	6.84	0.0336	0.076	0.00918	0.00333	11.3	428
	30.4	7.60	0.0381	0.083	0.0105	0.00343	11.6	475
0.118	23.5	5.88	0.0429	0.072	0.0113	0.00258	9.7	199
	26.5	6.62	0.0468	0.077	0.0123	0.00251	8.9	225
	29.5	7.38	0.0490	0.079	0.0133	0.00243	9.5	250
	32.5	8.13	0.0520	0.083	0.0143	0.00237	10.0	276
	35.5	8.87	0.0558	0.087	0.0159	0.00241	10.3	301
0.250	29.0	7.25	0.1030	0.095	0.0274	0.00239	8.0	116
	32.0	8.00	0.1020	0.094	0.0271	0.00215	8.5	128
	35.0	8.75	0.1050	0.096	0.0290	0.00211	8.9	140
	38.0	9.50	0.1190	0.106	0.0322	0.00215	8.8	152
0.250*	26.6	6.65	0.0936	0.088	0.0249	0.00238	7.2	106
	29.6	7.40	0.0930	0.087	0.0252	0.00217	8.1	118
	32.6	8.15	0.0950	0.089	0.0258	0.00201	8.8	130

* tests using a thinner boundary layer trip

≠ average of results on upper and lower surface

SYMBOLS

A'	factor used in collapsing three-dimensional friction measurements to two-dimensional theory
a	speed of sound
C_F	skin friction coefficient = friction drag per unit length ÷ $\pi q d$
C_{F_P}	theoretical skin friction coefficient for a flat plate
$\bar{C}_F$	$= C_F \div \left[1 + \frac{0.017\ \ell/d}{(R_e)^{1/5}}\right]$
d	wire diameter
d^*	$d \cdot \frac{a}{\nu} \cdot \frac{\nu_o}{a_o}$
D	cross flow force per unit length of wire
F	friction force per unit length of wire
f	frequency of boundary shedding from one side
h	depression of target below towing aircraft
ℓ	distance along wire from target
M	Mach number in free stream
n	exponent of the boundary layer velocity profile given by $\frac{v}{V} = \left(\frac{y}{\delta}\right)^{1/n}$
q	kinematic pressure = $\frac{1}{2} \rho V^2$
r	$\tan \alpha_o / \tan \alpha_\infty$
S	maximum body area normal to the cross flow
s	Strouhal number
T	wire tension
v	velocity at a point within the boundary layer parallel to the wire surface
V	free stream velocity
ω	weight per unit length of wire
y	radial distance measured from centreline of wire
C, P, Q, R	constants for a given towing system (section 4.3)
α	local wire incidence
δ	boundary layer displacement thickness
ν	kinematic viscosity of the free stream air
ρ	density of the free stream air

SYMBOLS (Contd.)

Suffices

o	value at ground level (a, ν)
o	value at target (T, α)
∞	value as $\ell \to \infty$
c	cross flow component

REFERENCES

No.	Author	Title, etc.
1	M.B. Glauert M.J. Lighthill	The axi-symmetric boundary layer on a long thin cylinder. Proceedings of a Symposium on Boundary Layer Effects in Aerodynamics. N.P.L. (1955)
2	G.W.H. Stevens	Factors effecting the design of a system for towing a body on a long length of wire. R.A.E. Technical Note Mech. Eng. 335 (ARC 24644) (1961)
3	J. Nikuradse	Geselzmässigkeiten der turbulenten Strömung in glatten Rohren. Forschungs-Arb. Ing. Wessen, No.356 (1932)
4	H. Schlichting	Boundary layer theory. Pergamon Press Ltd. (1955)
5	S.F. Hoerner	Fluid dynamic drag, published by the author, p.17-4 (1965)
6	H.U. Eckert	Simplified treatment of the turbulent boundary layer along a cylinder in compressible flow. J. Aero. Sc. (1952)
7	G. Hughes	Friction and form resistance in turbulent flow, and a proposed formulation for use in model and ship correlation. Inst. Nav. Arch. pp.314-376 (1954)
8	K.D. Thompson D.F. Morrison	On the asymmetric shedding of vortices from slender cylindrical bodies at large angles of yaw. Weapons Research Establishment, Australia Technical Note H.S.A. 106 (1965)
9	H.J. Allen	Estimation of the forces and moments acting on inclined bodies of revolution of high fineness ratio. NACA RM/A9126 (TIB 2289) (1949)
10	P. Bragg T.P. Cripps B.S. Grieve	Meteor TT Mk.20 - performance and handling trials with a Rushton towed target system. Report AAEE/817/6 (Part 4) (1966)

REFERENCES (Contd.)

No.	Author	Title, etc.
11	P. Bragg J.D. Eagles I.W. Kitchin	AAEE unpublished report
12	W.L. Bartlett	Drag and compatibility test of the TDU-4/B target with the B57E external lightweight tow system. APGC-TR-59-39 (1959)

ATTACHED:-

Drgs. 005/905839 to 005/905864
Negs. C4976 to 4977

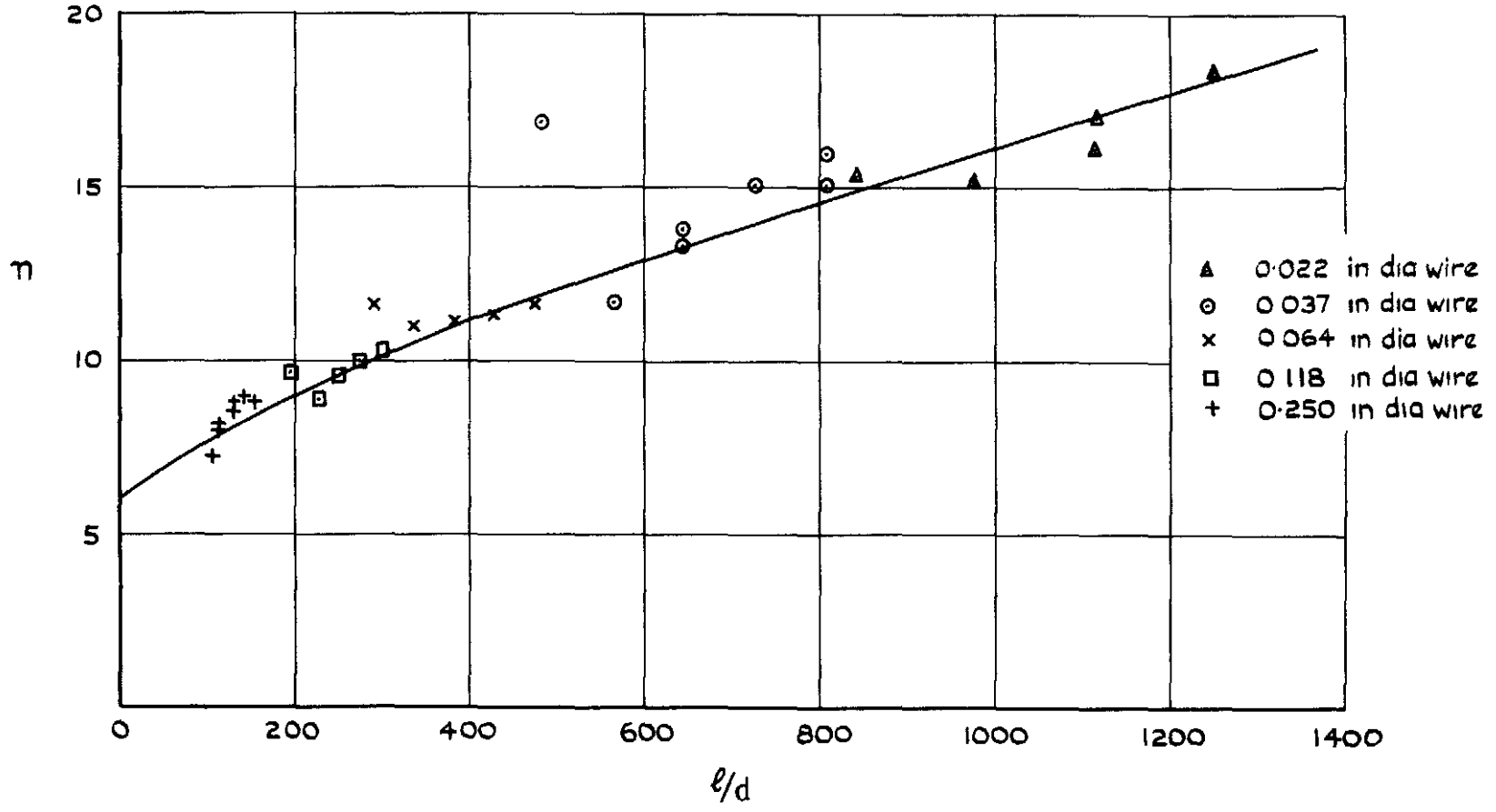

Fig. 1 Effect of ℓ/d on velocity profile exponent, n

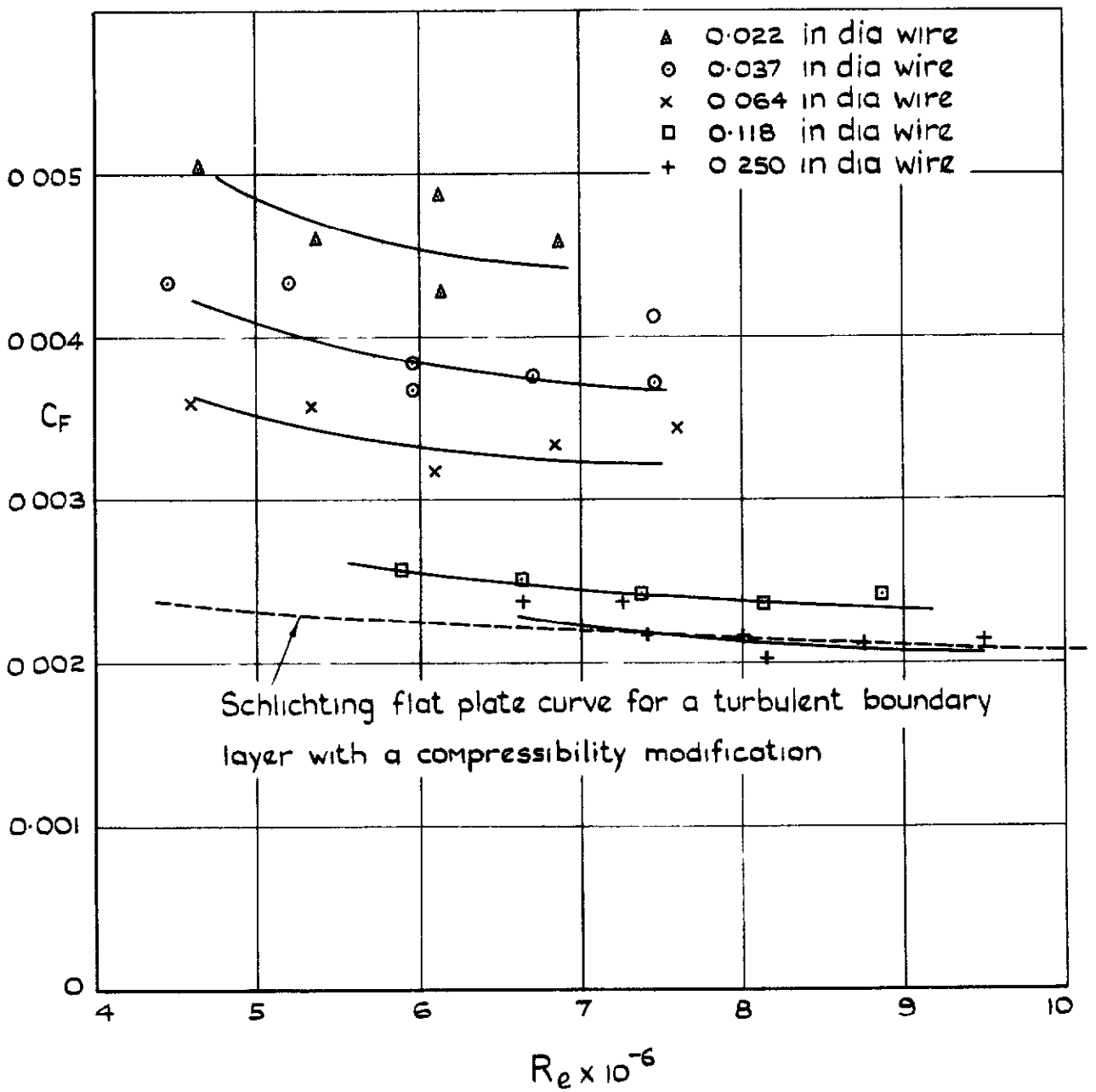

Fig 2 Mean skin friction coefficient on wires

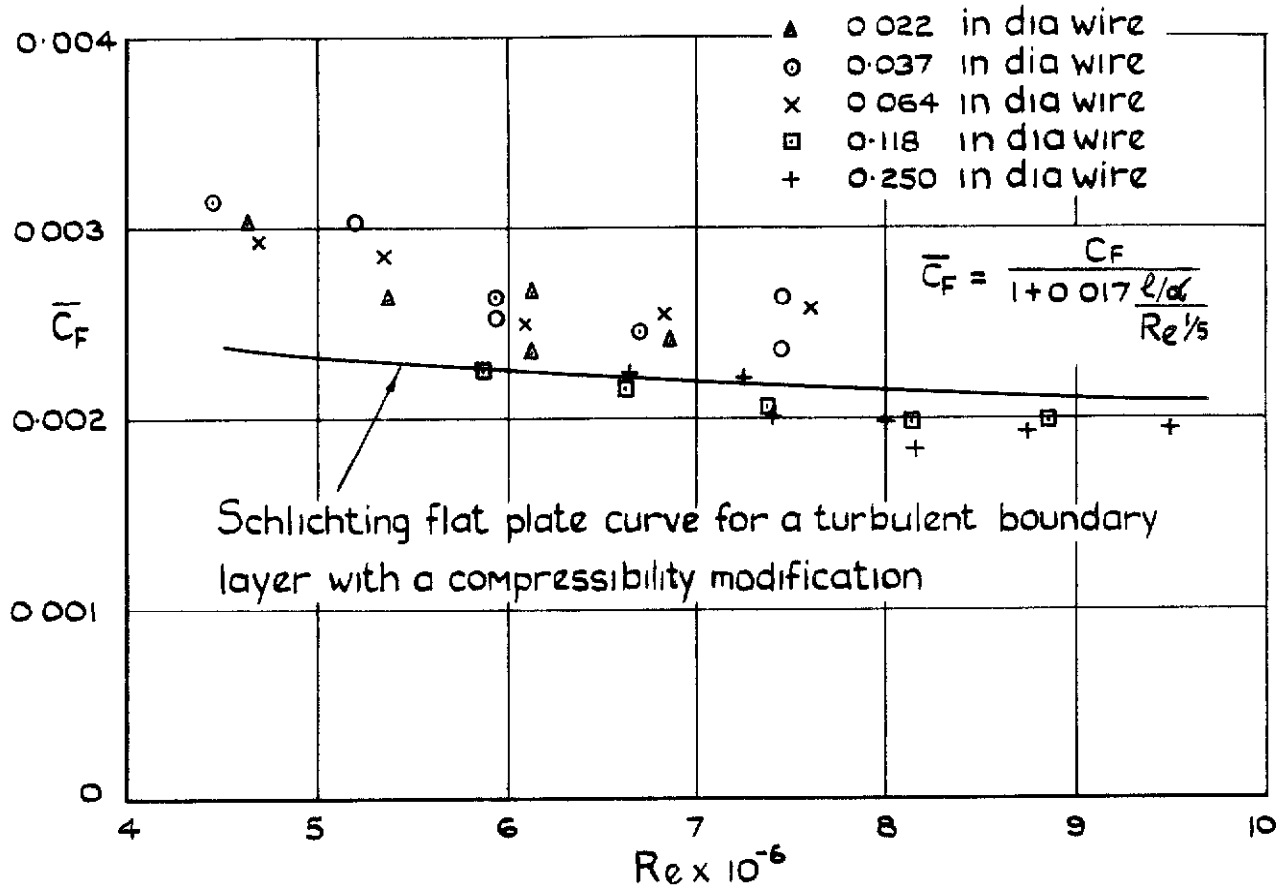

Fig. 3 Comparison of $C_{F_{PL}}$ and $\bar{C}_F$ where $\bar{C}_F$ is obtained from the C_F data by a three-dimensional correction factor

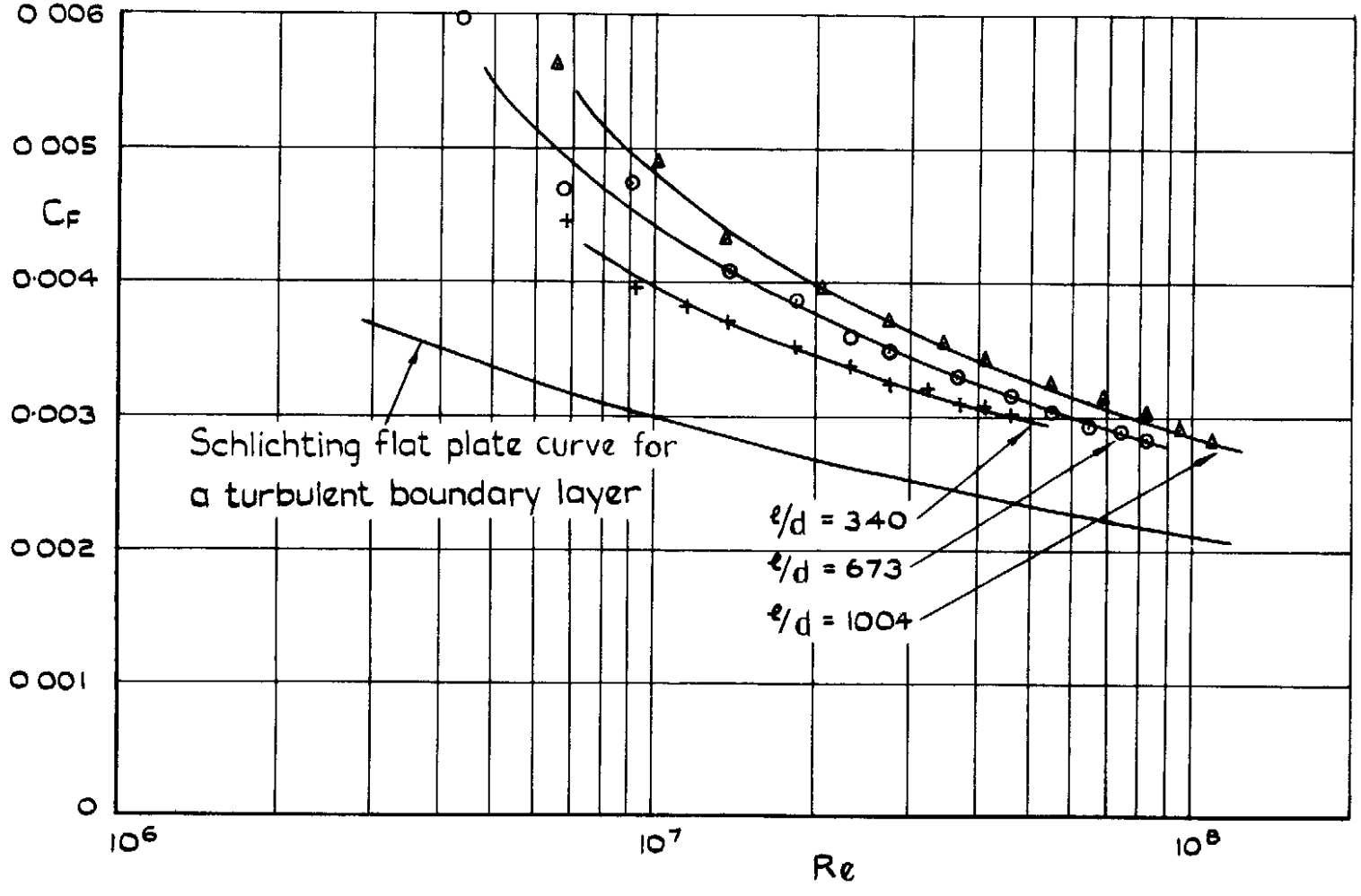

Fig. 4 Skin friction of cylinders in water

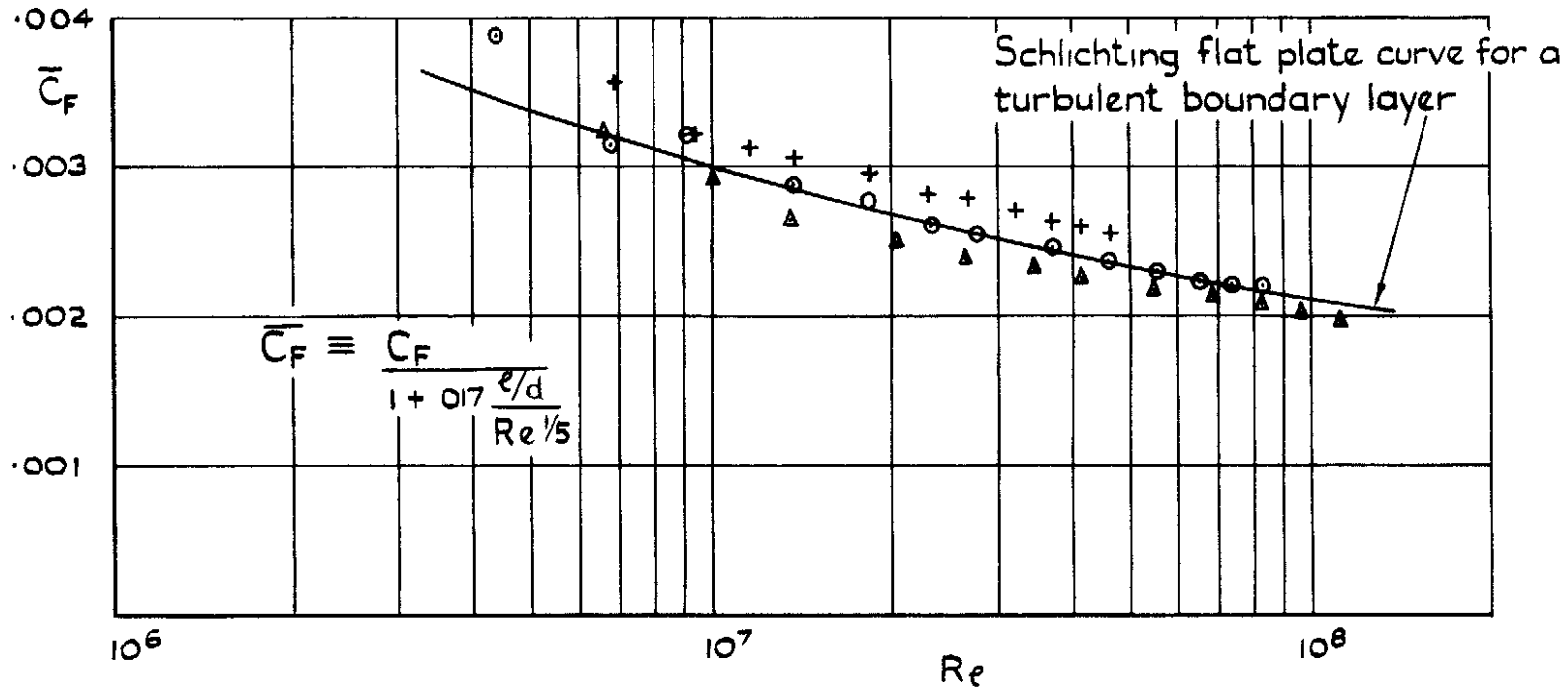

Fig. 5 Comparison of $\bar{C}_F$ and $C_{F_{PL}}$ for cylinders in water

Calculated for $\begin{cases} M = 1.6 \\ \text{Altitude} = 25000 \text{ ft} \\ d = 0.05 \text{ in} \\ \frac{\partial Re}{\partial \ell} = 0.424 \times 10^6/\text{in} \end{cases}$

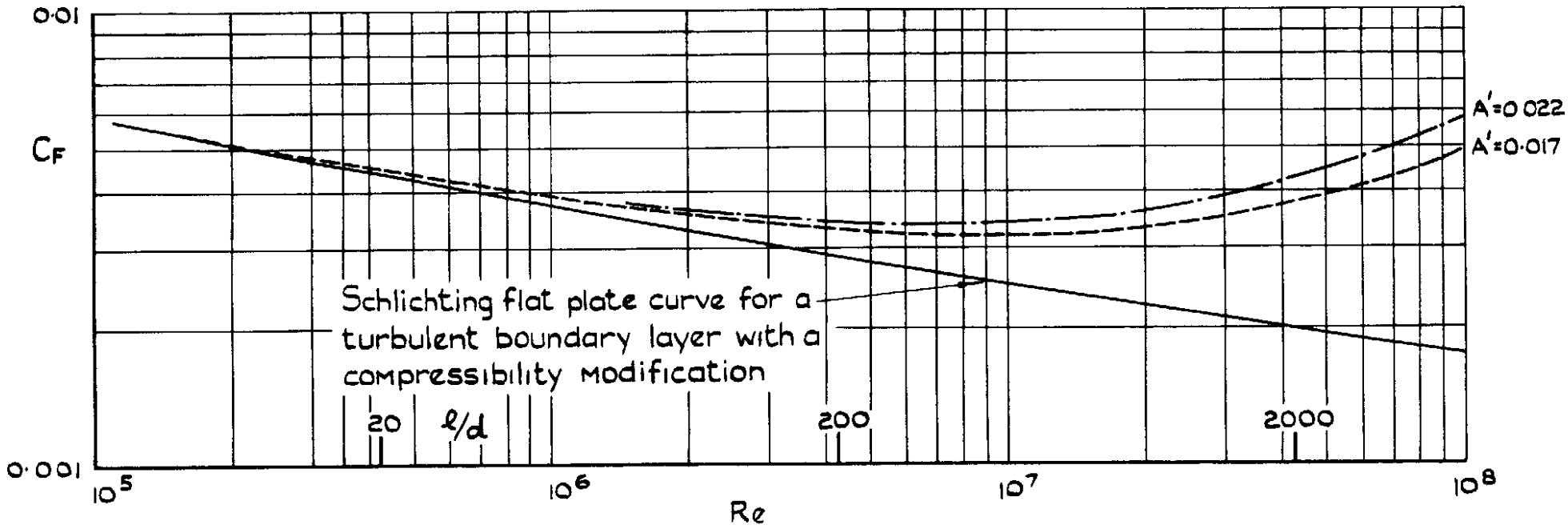

Fig. 6 Typical curves showing effect of ℓ on C_F of wire compared to that of a flat plate for turbulent boundary layer

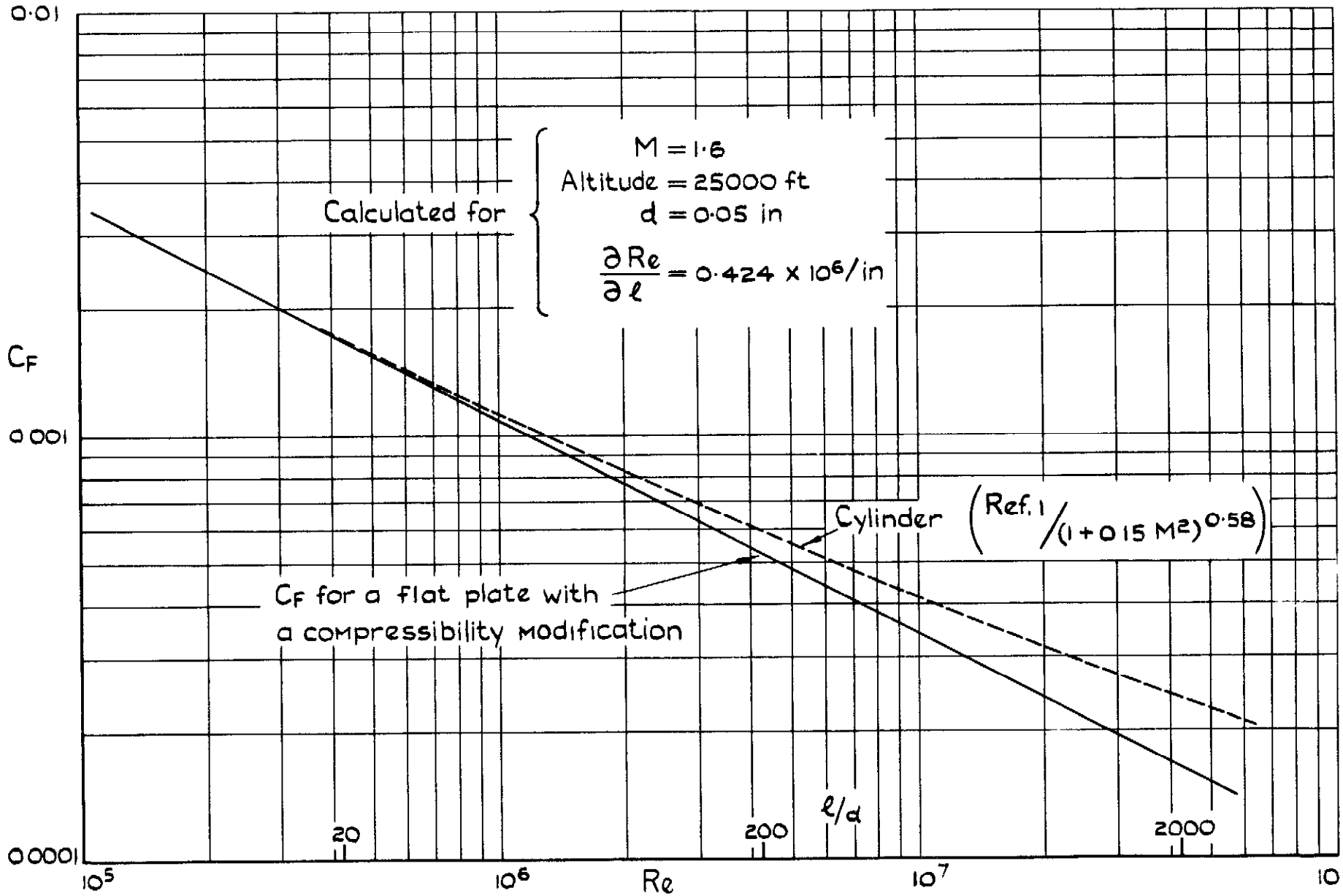

Fig. 7 Typical curves showing effect of ℓ on C_F of wire compared to that of a flat plate for laminar boundary layer

¼in. dia. rod, α=25° M=1.50

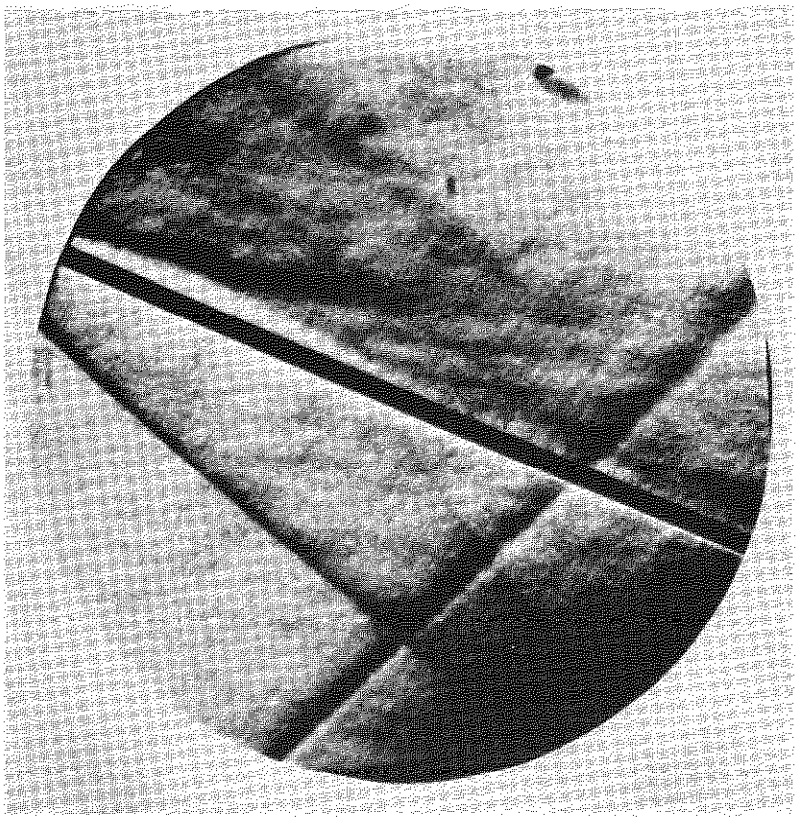

Continuous source schlieren

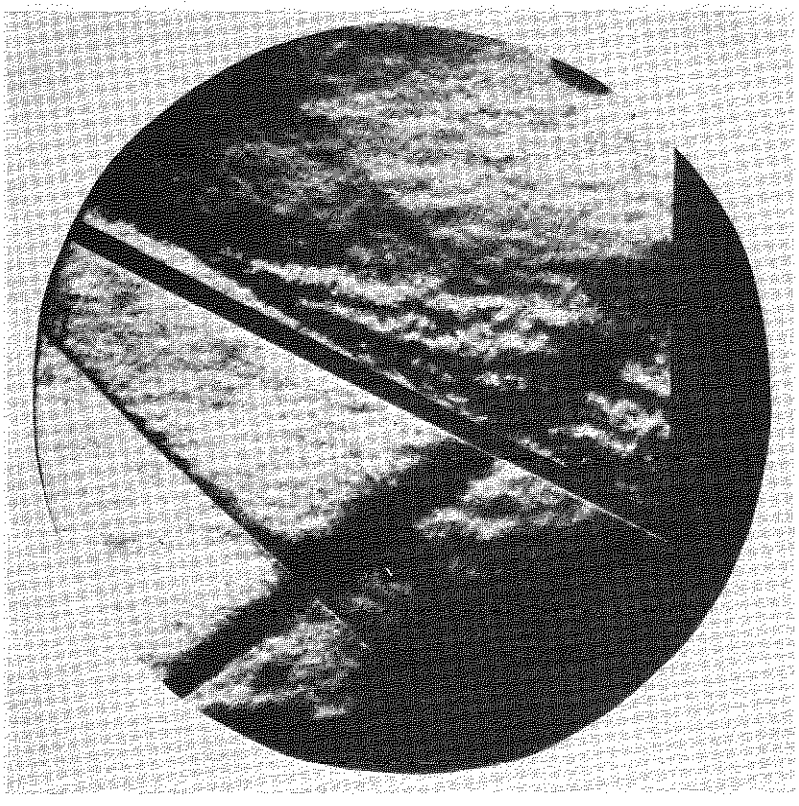

Spark schlieren

Fig.8 Schlieren photographs of rod at incidence

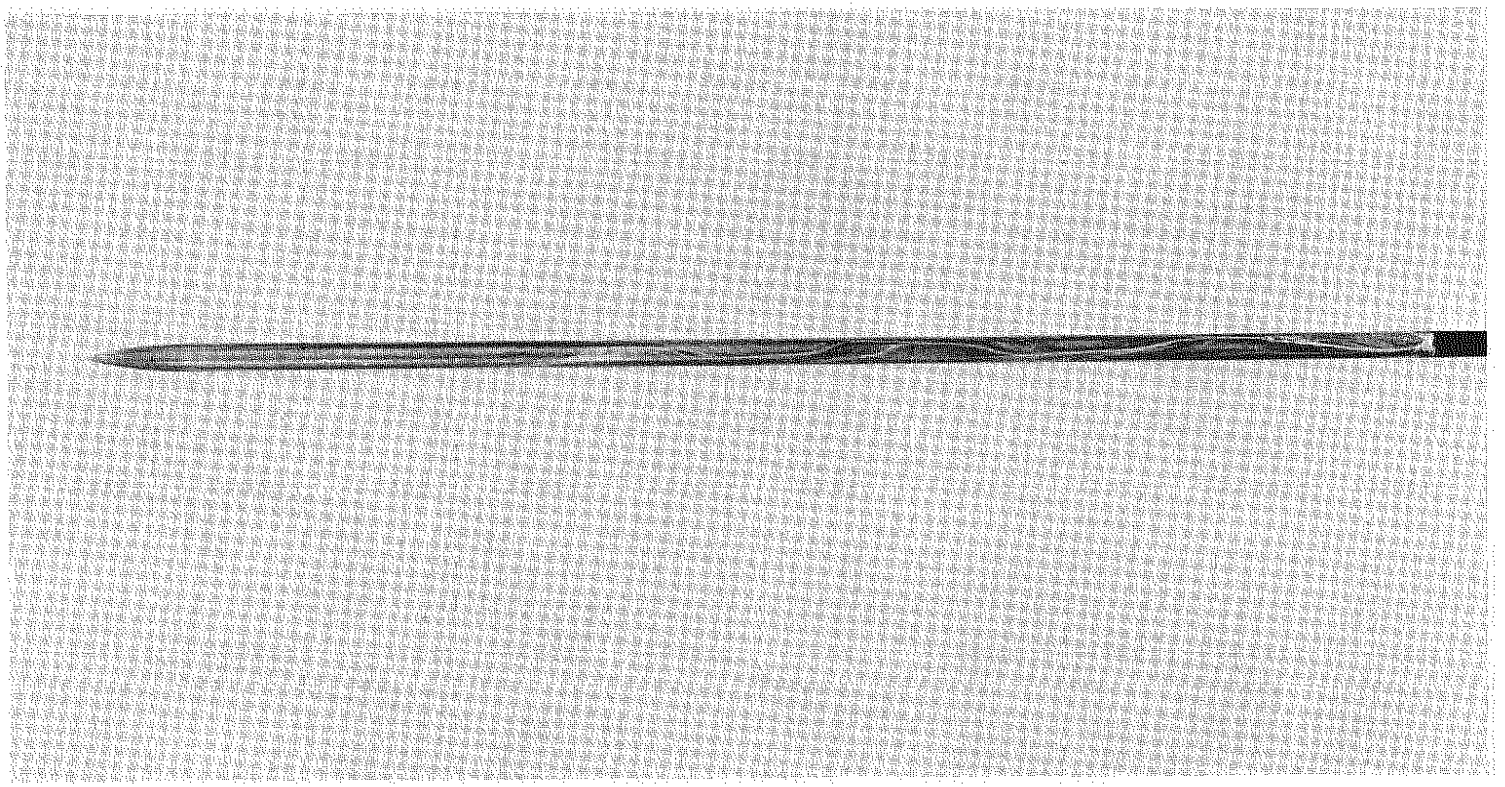

Fig.9 Oil flow pattern on rear facing surface of rod at incidence

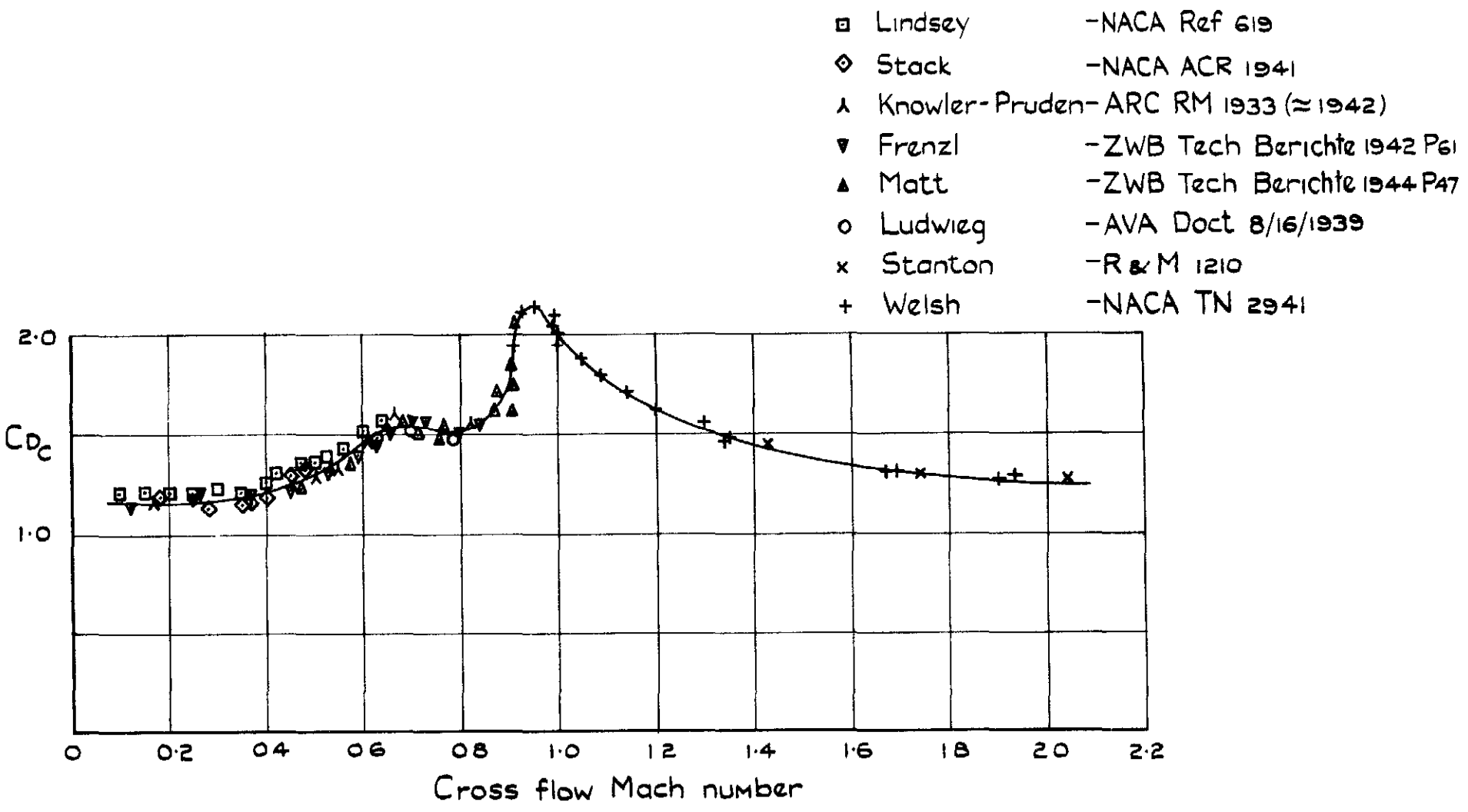

Fig. 10 Drag coefficients of circular cylinders normal to the stream direction

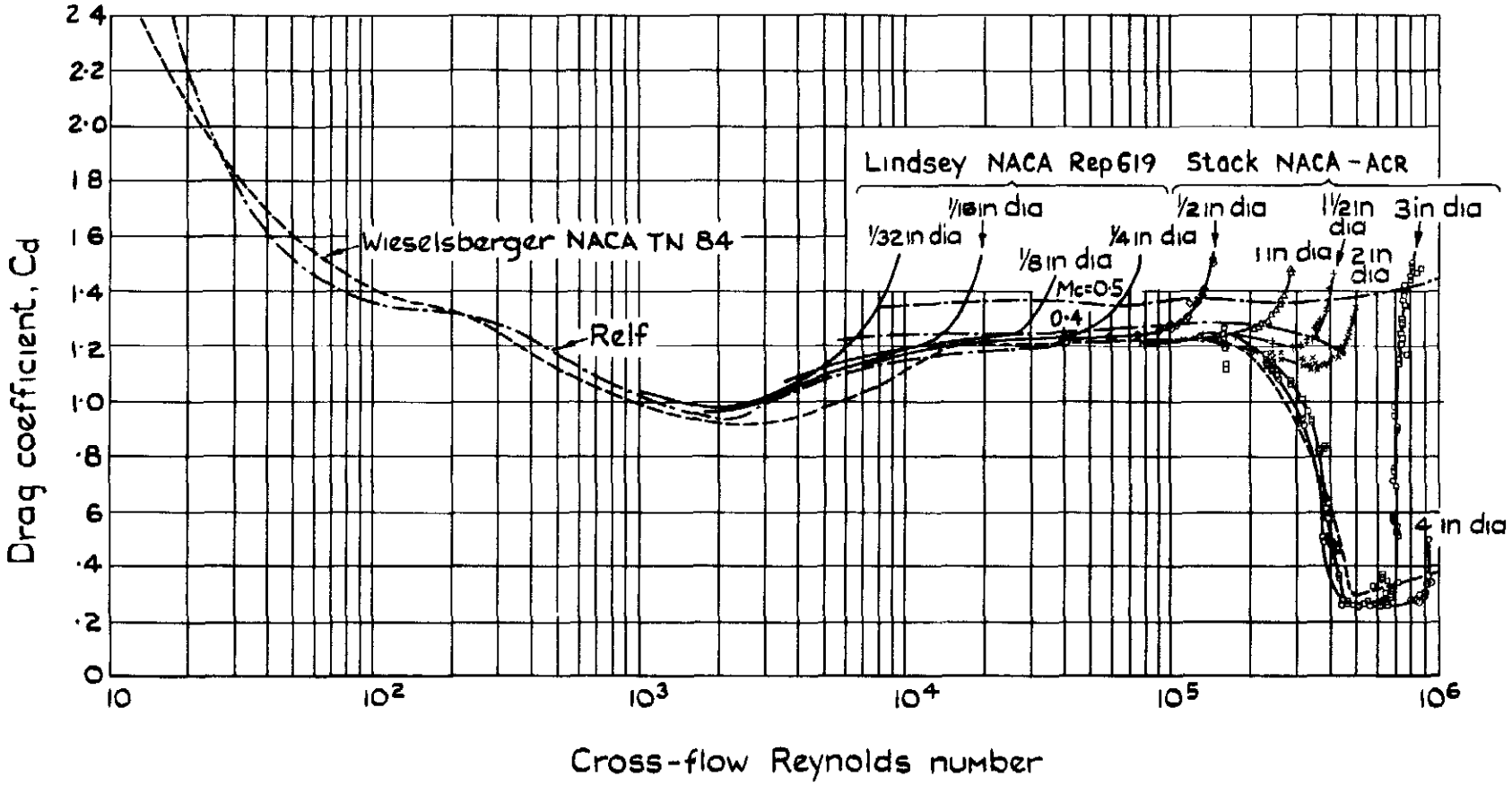

Fig. 11 Circular cylinder drag coefficient as a function of Reynolds number

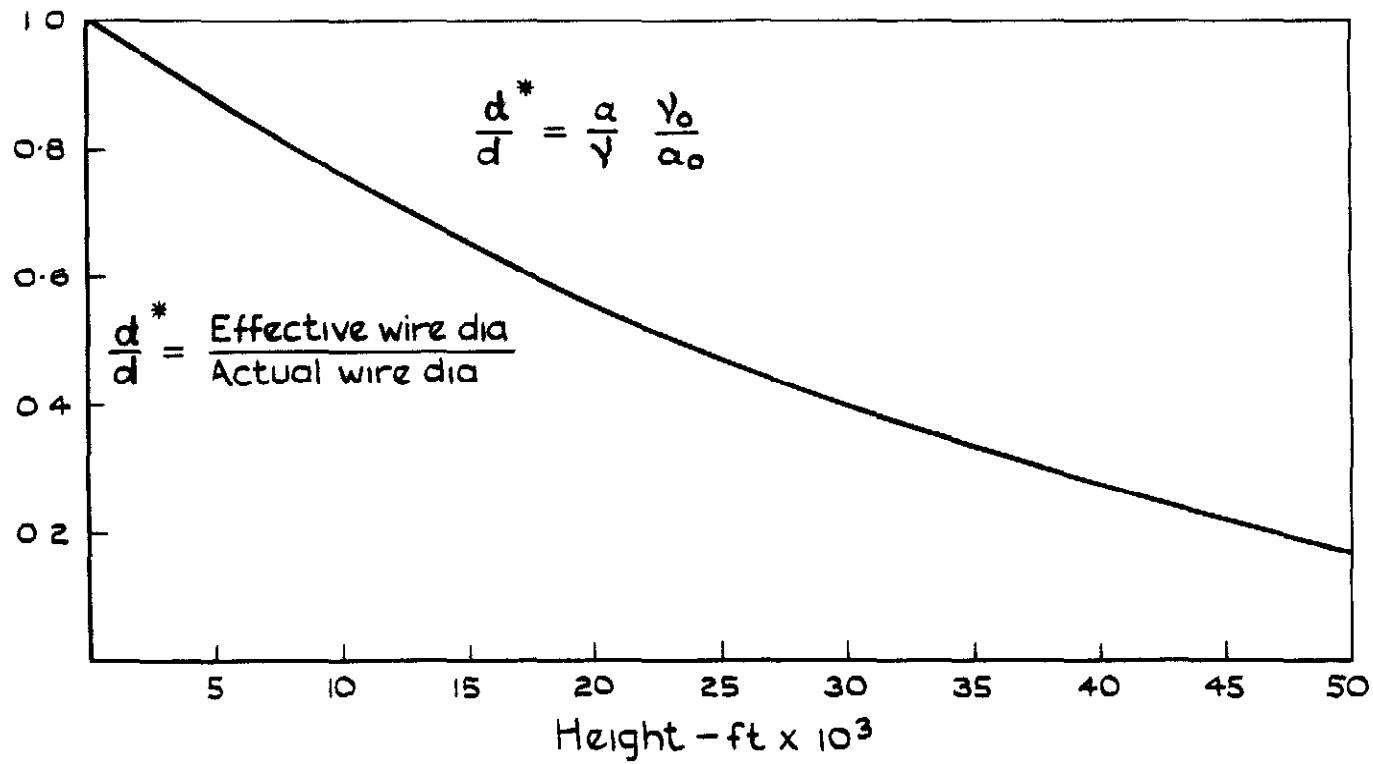

Fig. 12 Variation of "Effective" wire dia for skin friction estimates

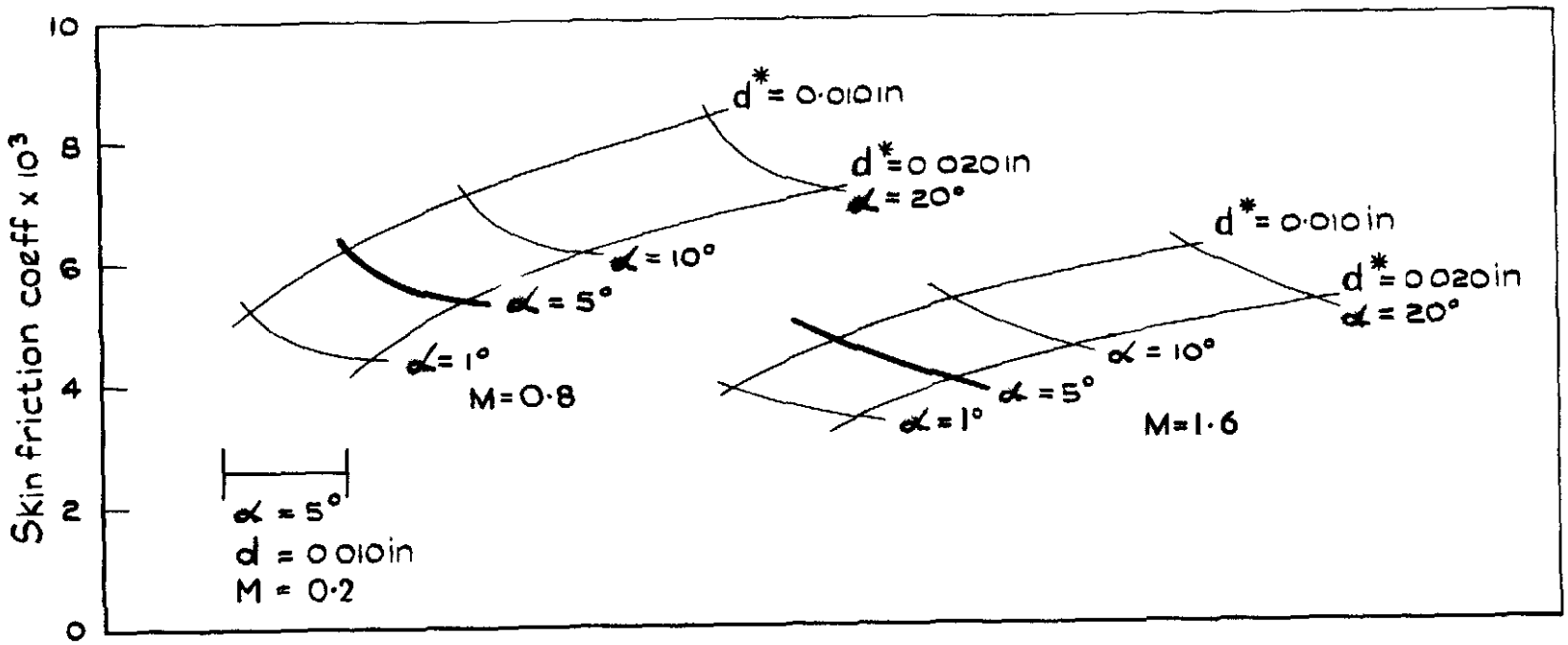

Fig. 13 Estimated local skin friction coefficient for wires

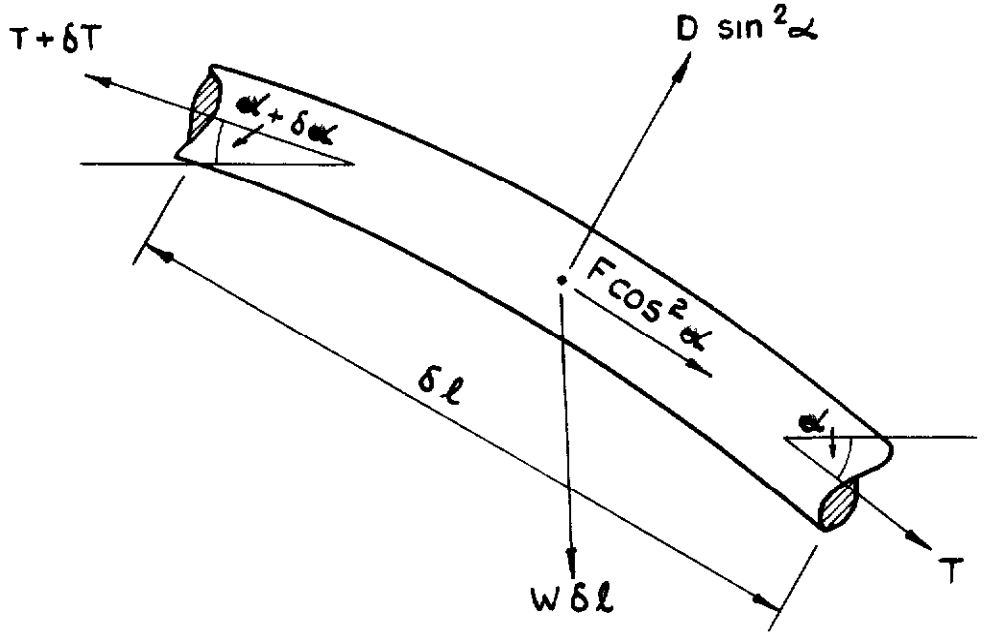

Fig. 14 Forces on element of wire

$$I_1 = \frac{\sin \alpha_\infty}{1+\cos^2 \alpha_\infty}\left\{\log\left|\frac{(1+\cos\alpha_\infty)\tan \alpha/2 + \sin\alpha_\infty}{(1+\cos\alpha_\infty)\tan \alpha/2 - \sin\alpha_\infty}\right| - 2\cos\alpha_\infty \tan^{-1}\left[\frac{(1-\cos\alpha_\infty)}{\sin\alpha_\infty}\tan \alpha/2\right]\right\}_{\alpha_0}^{\alpha}$$

$$I_{1(\text{approx})} = \frac{\tan\alpha_\infty}{2}\log\left|\frac{\tan\alpha + \tan\alpha_\infty}{\tan\alpha - \tan\alpha_\infty}\right|_{\alpha_0}^{\alpha}$$

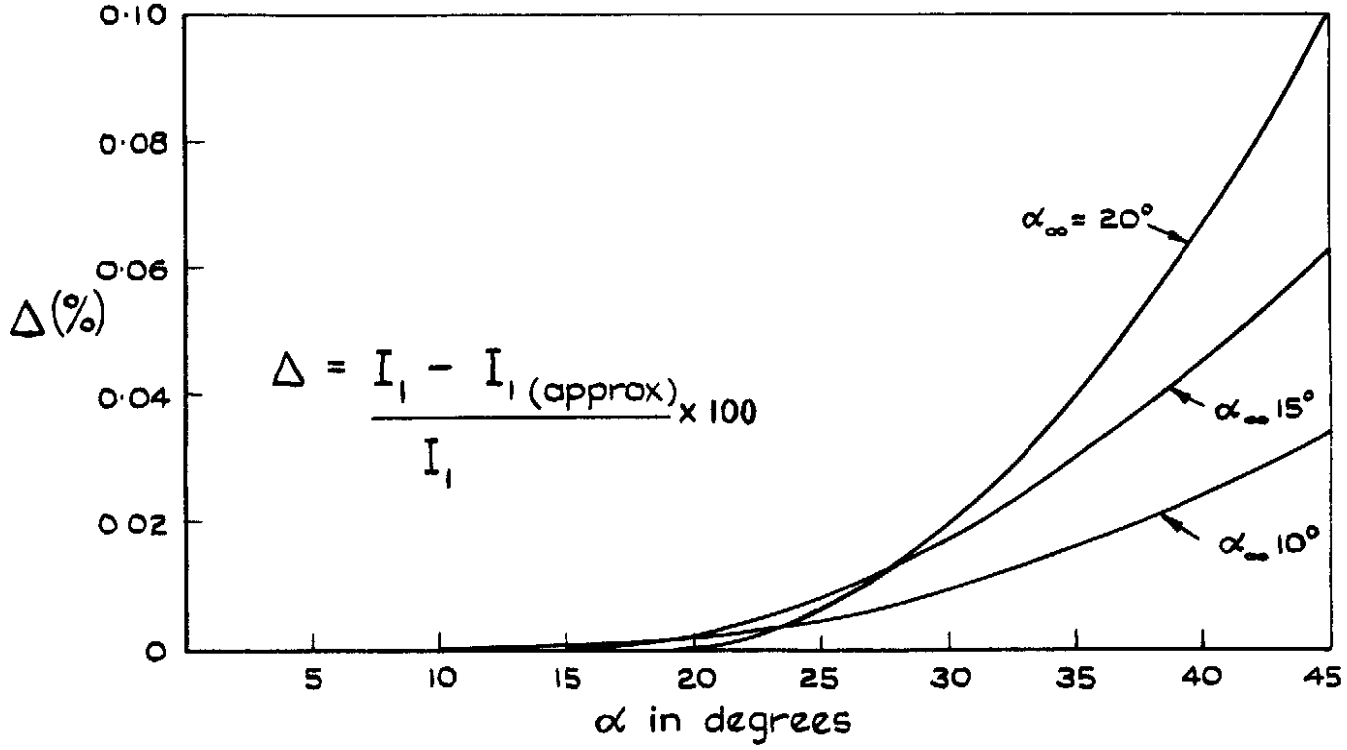

Fig. 15

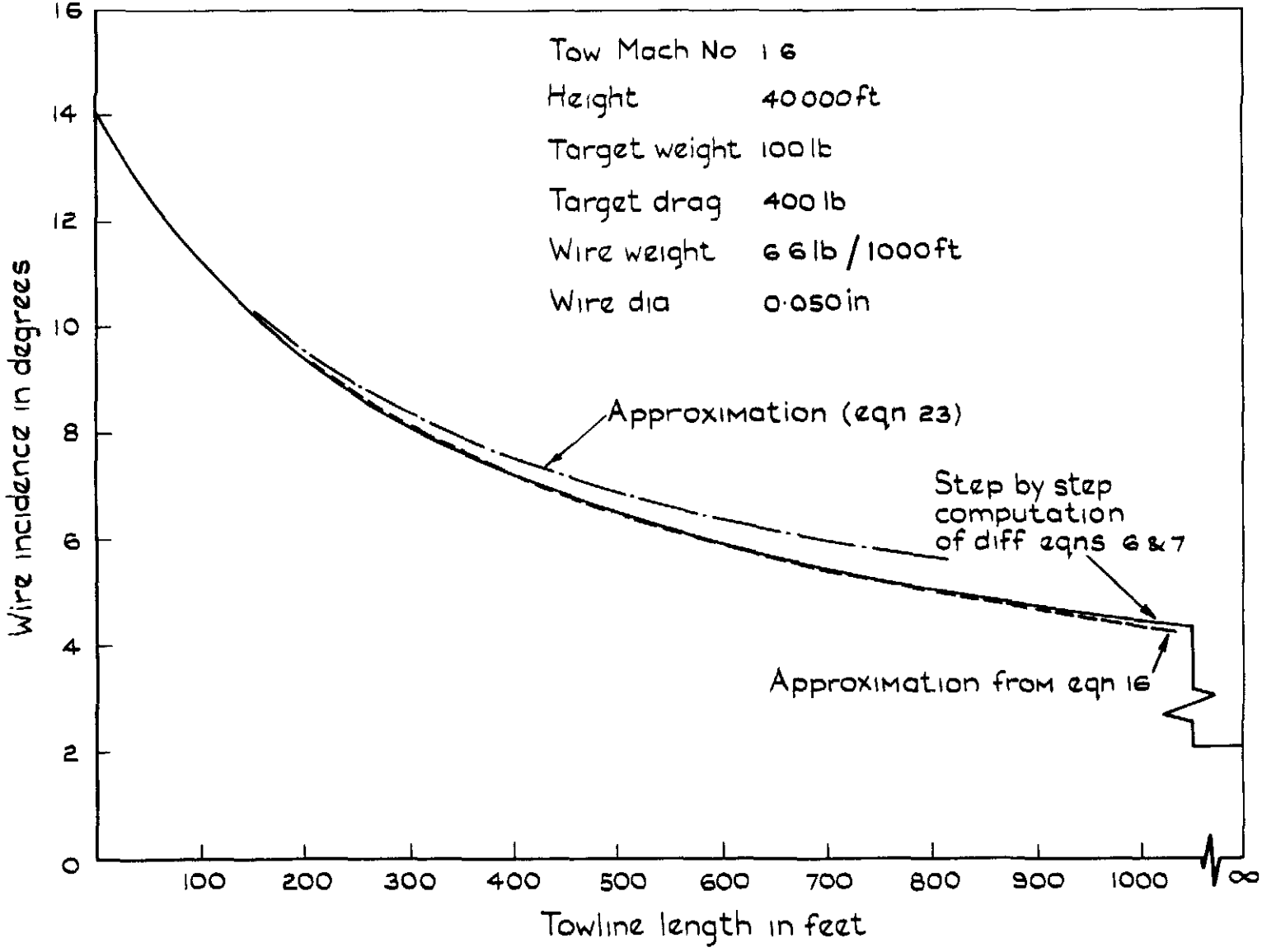

Fig. 16 Comparison of exact and approximate incidence distribution

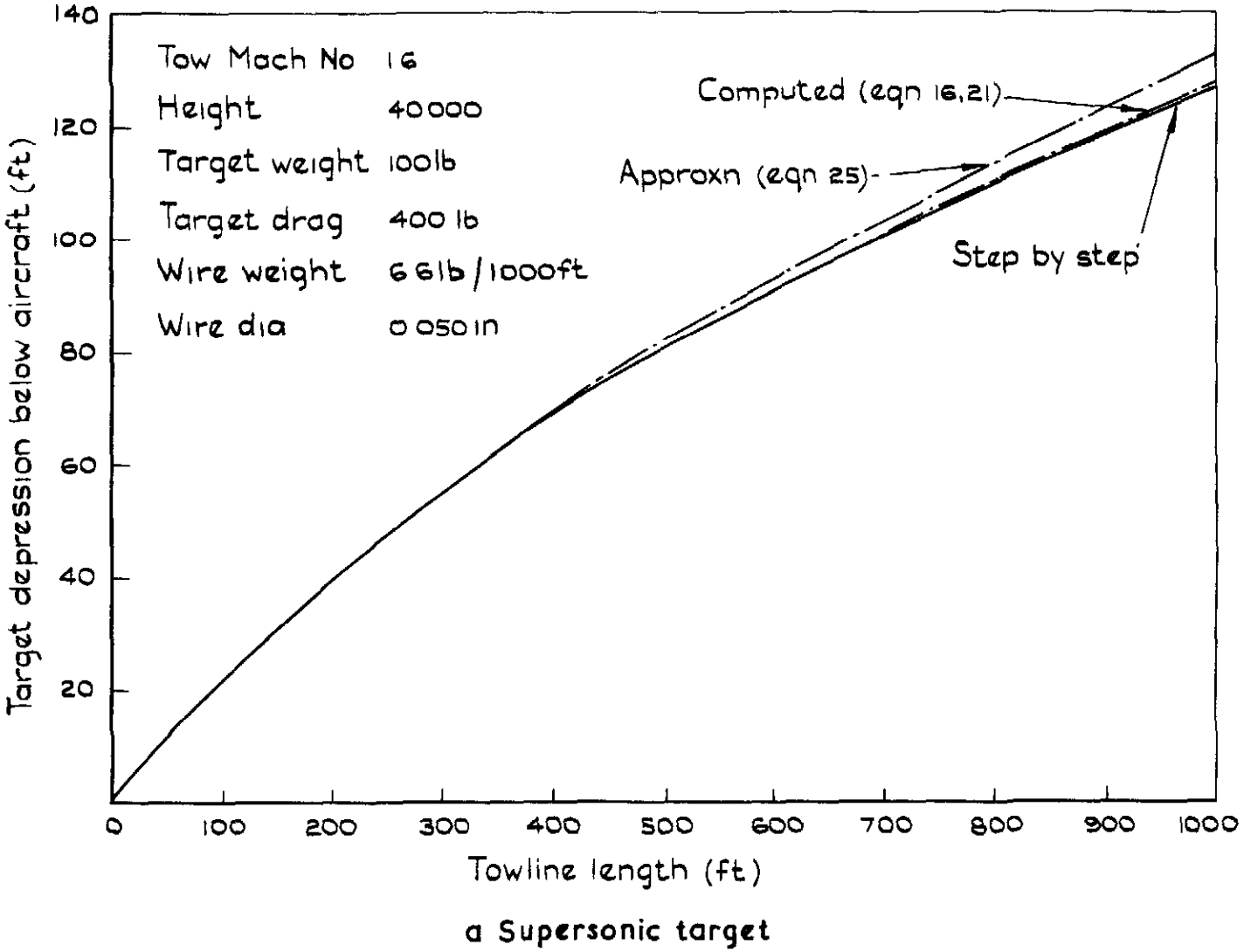

Fig. 17 Estimated terminal wire shape

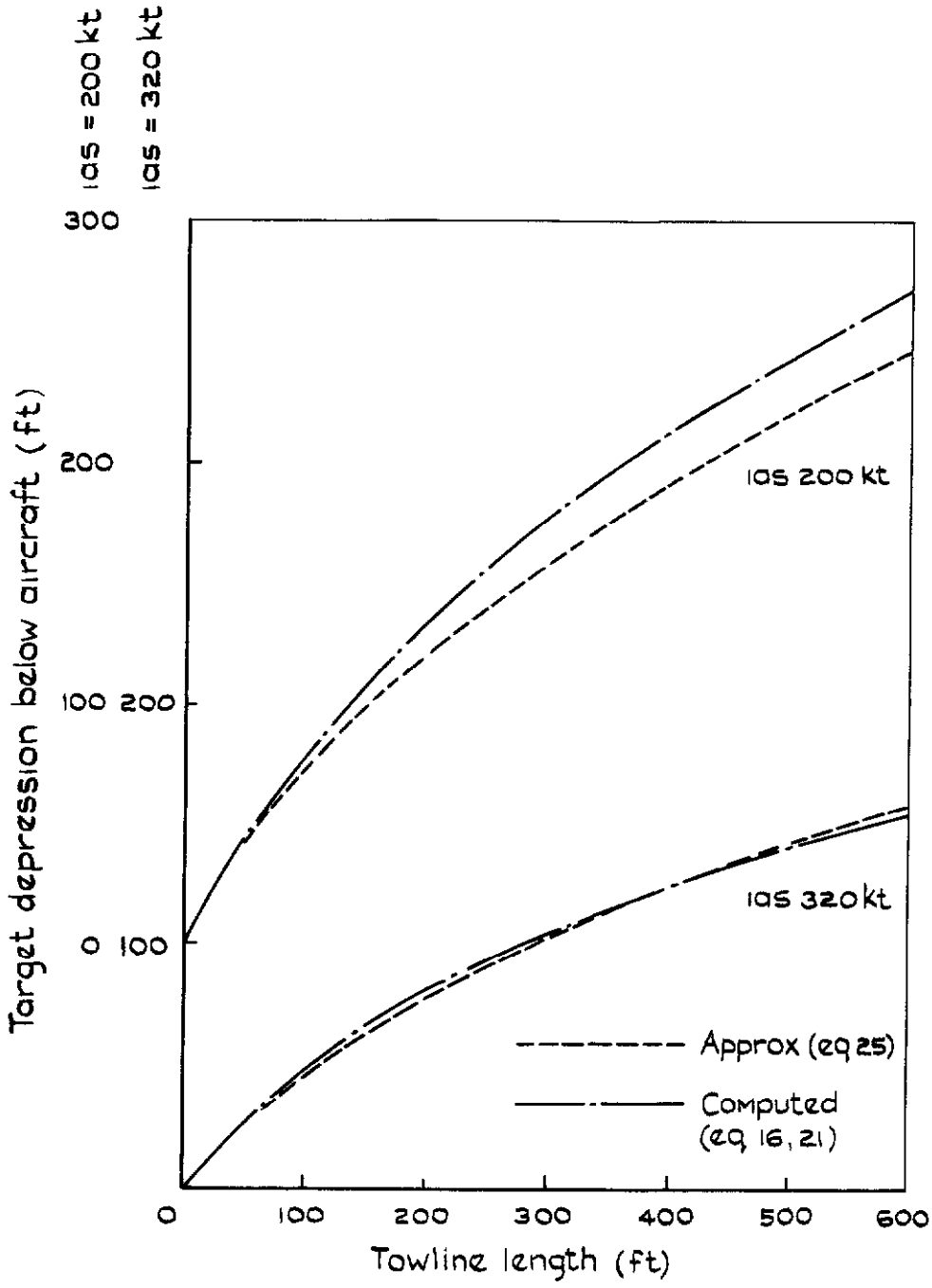

b Flights of refs 10, 11

Fig. 17 contd

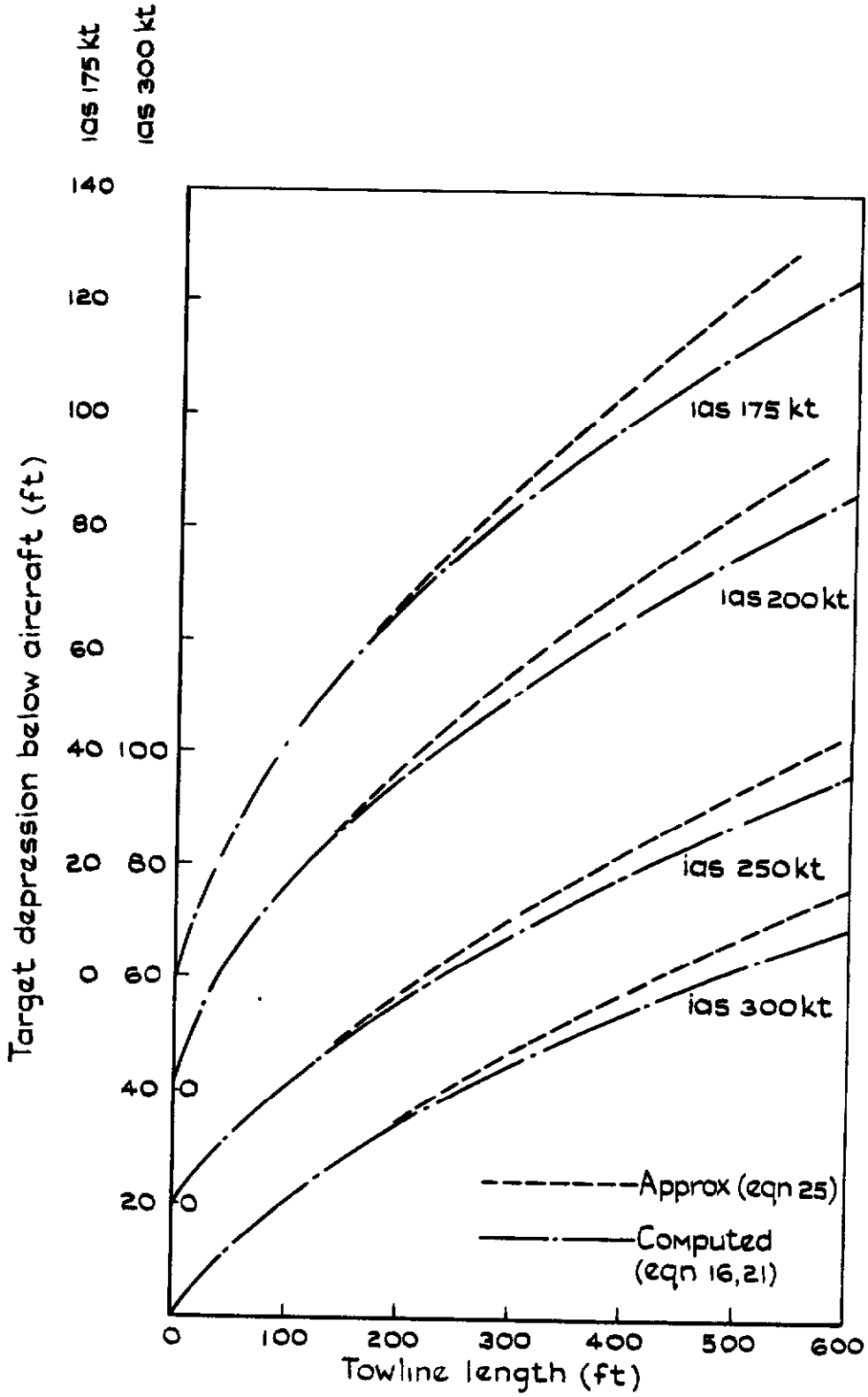

c Flights of ref 12

Fig. 17 concld

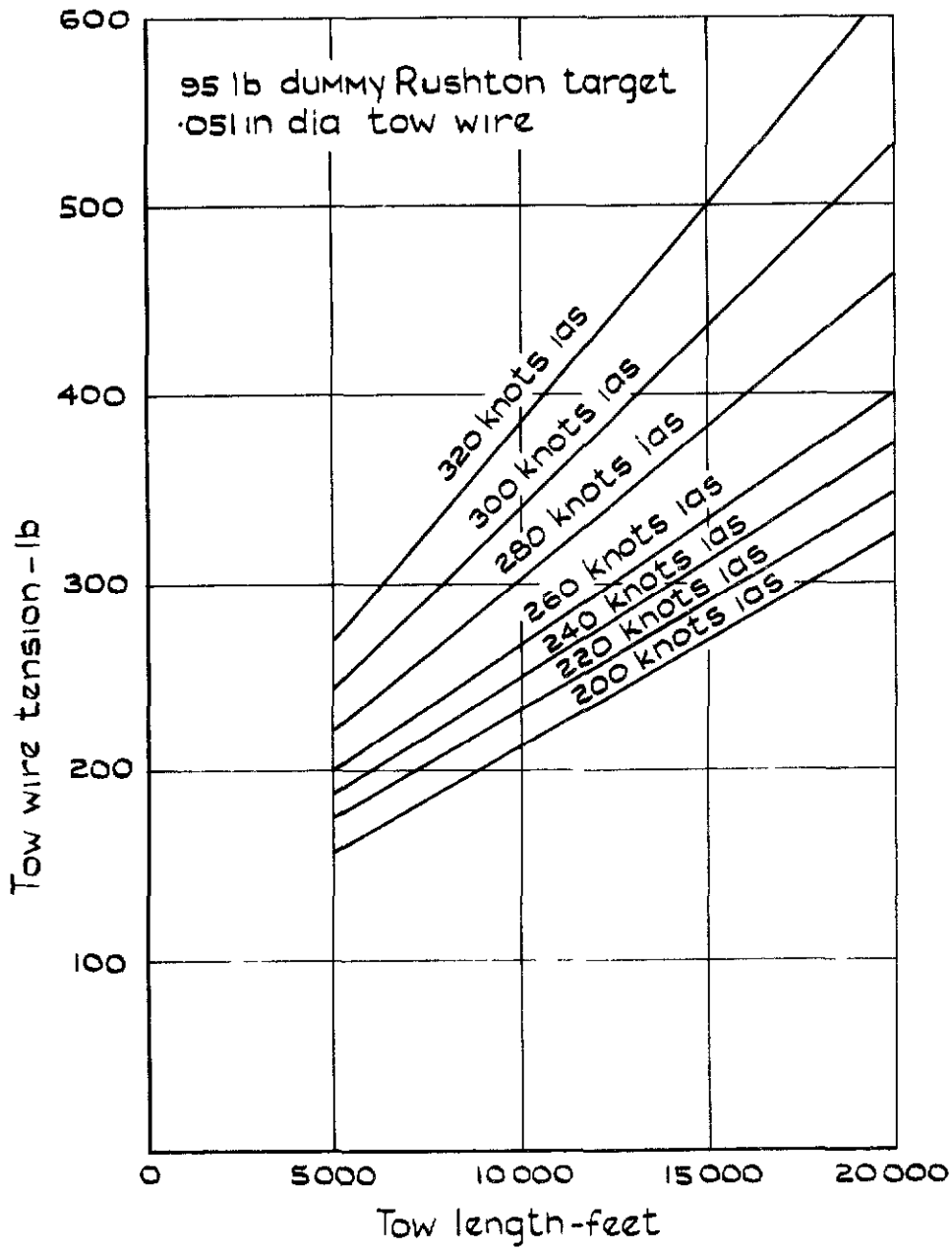

a From ref 10

Fig 18 Tow wire tension at various indicated air speeds & tow lengths

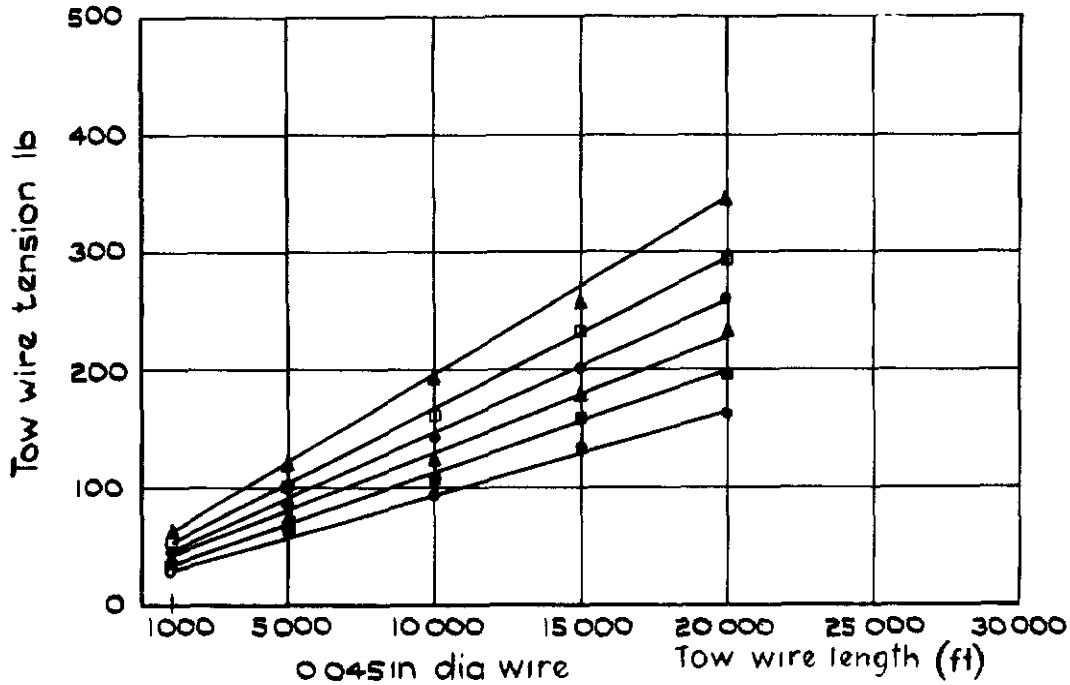

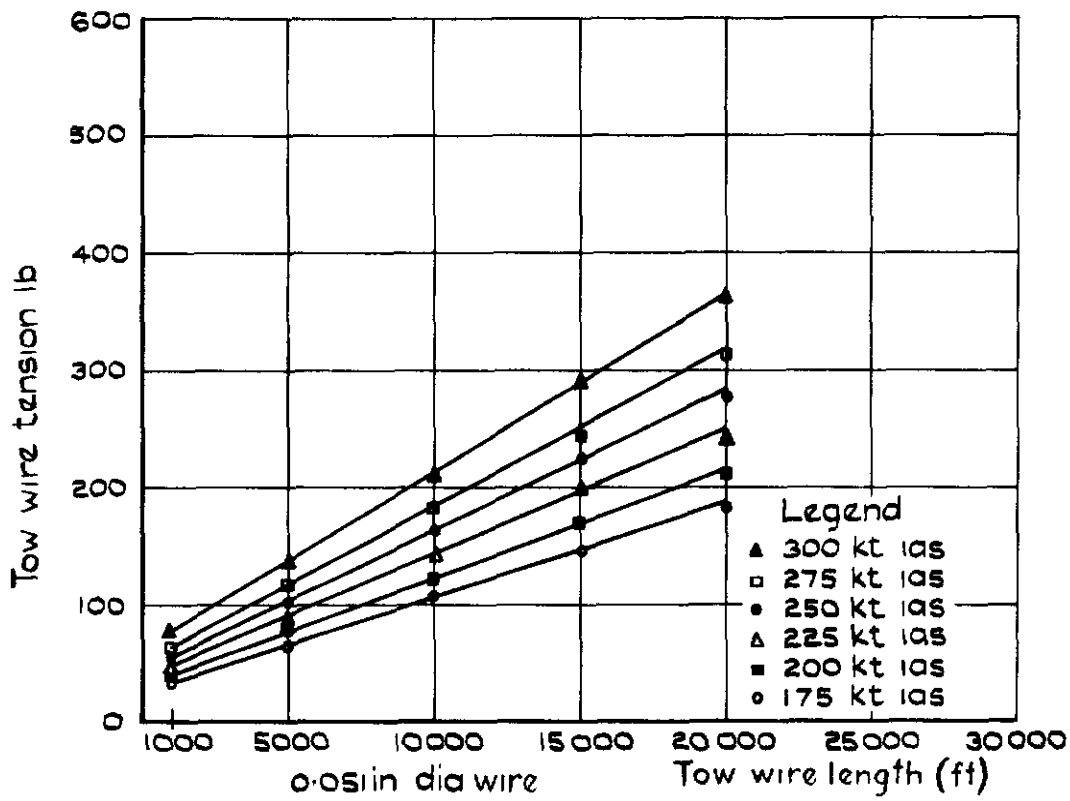

b From ref 12

Fig. 18 contd

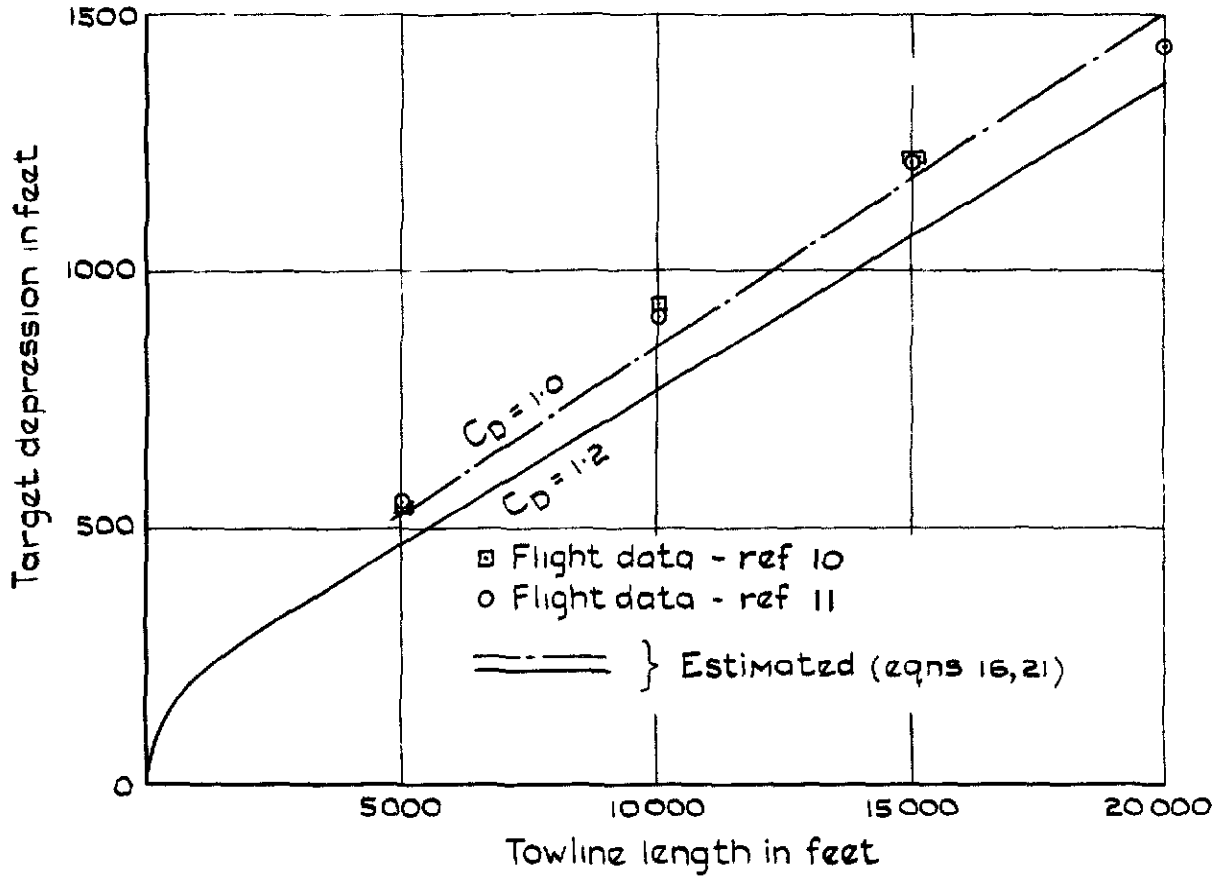

a ias 320kt

Fig. 19 Comparison with flight data (ref. 10, 11)

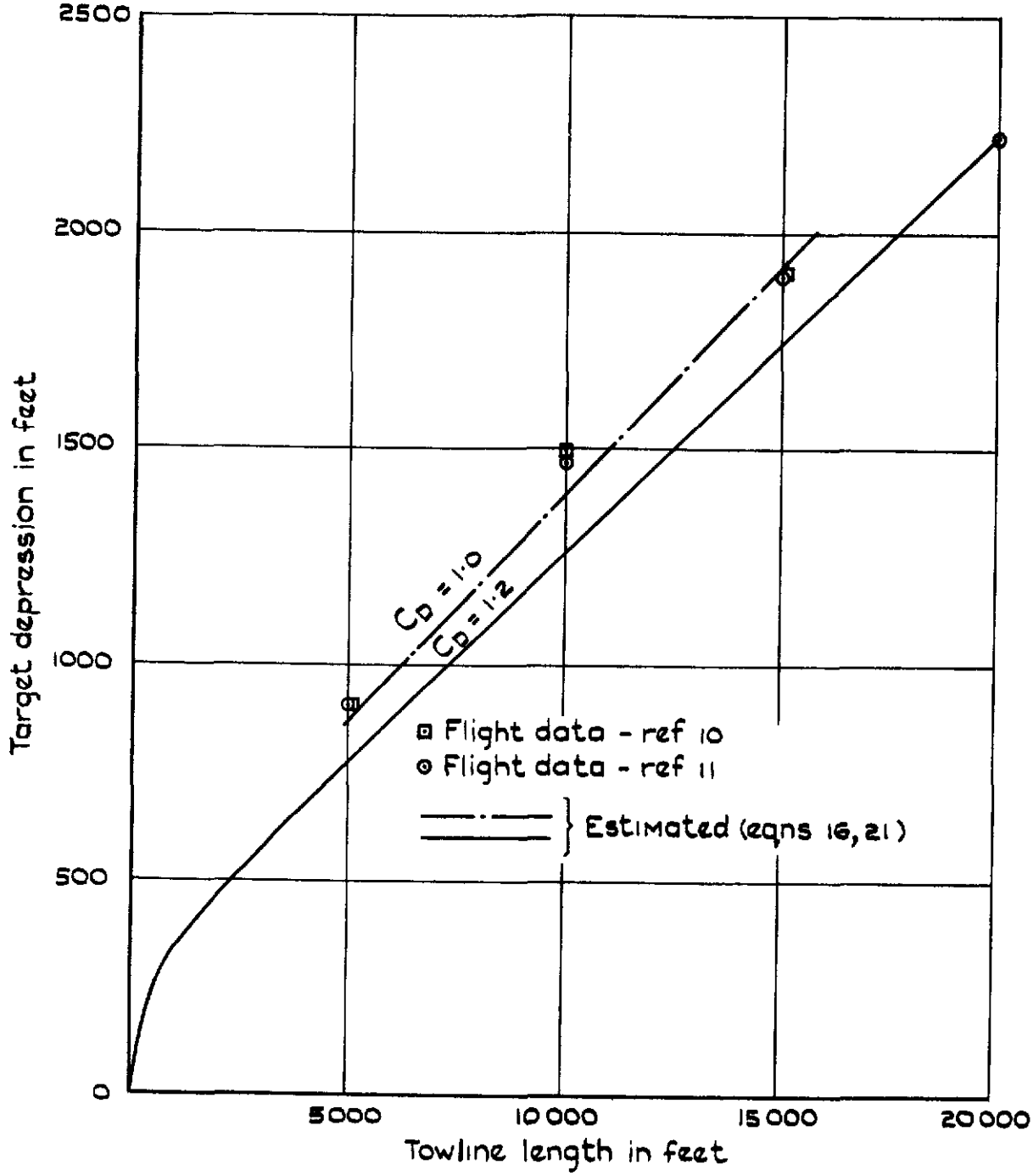

b ias 200kt

Fig. 19 contd

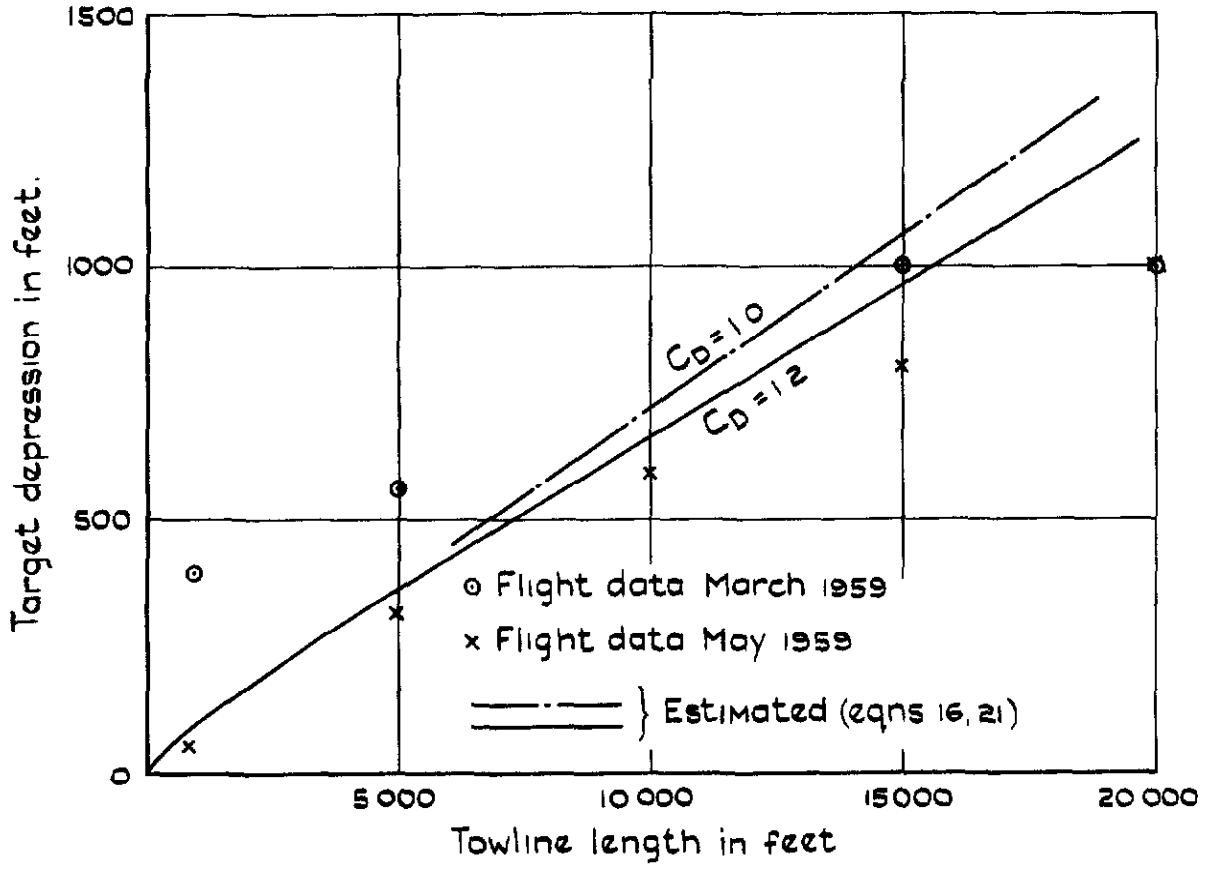

a ias 300 kt

Fig. 20 Comparison with flight data (ref 12)

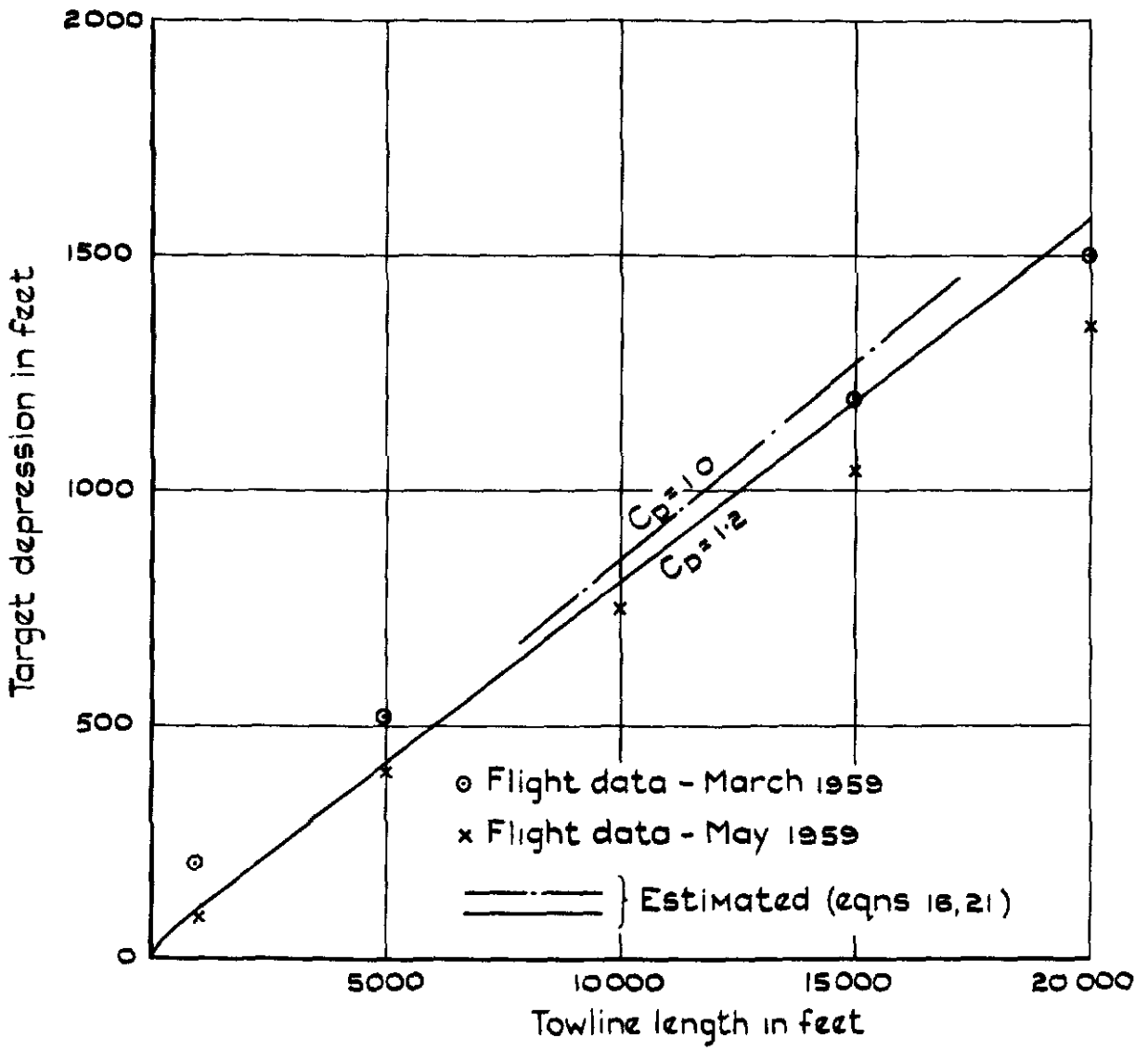

b las 250kt

Fig. 20 contd

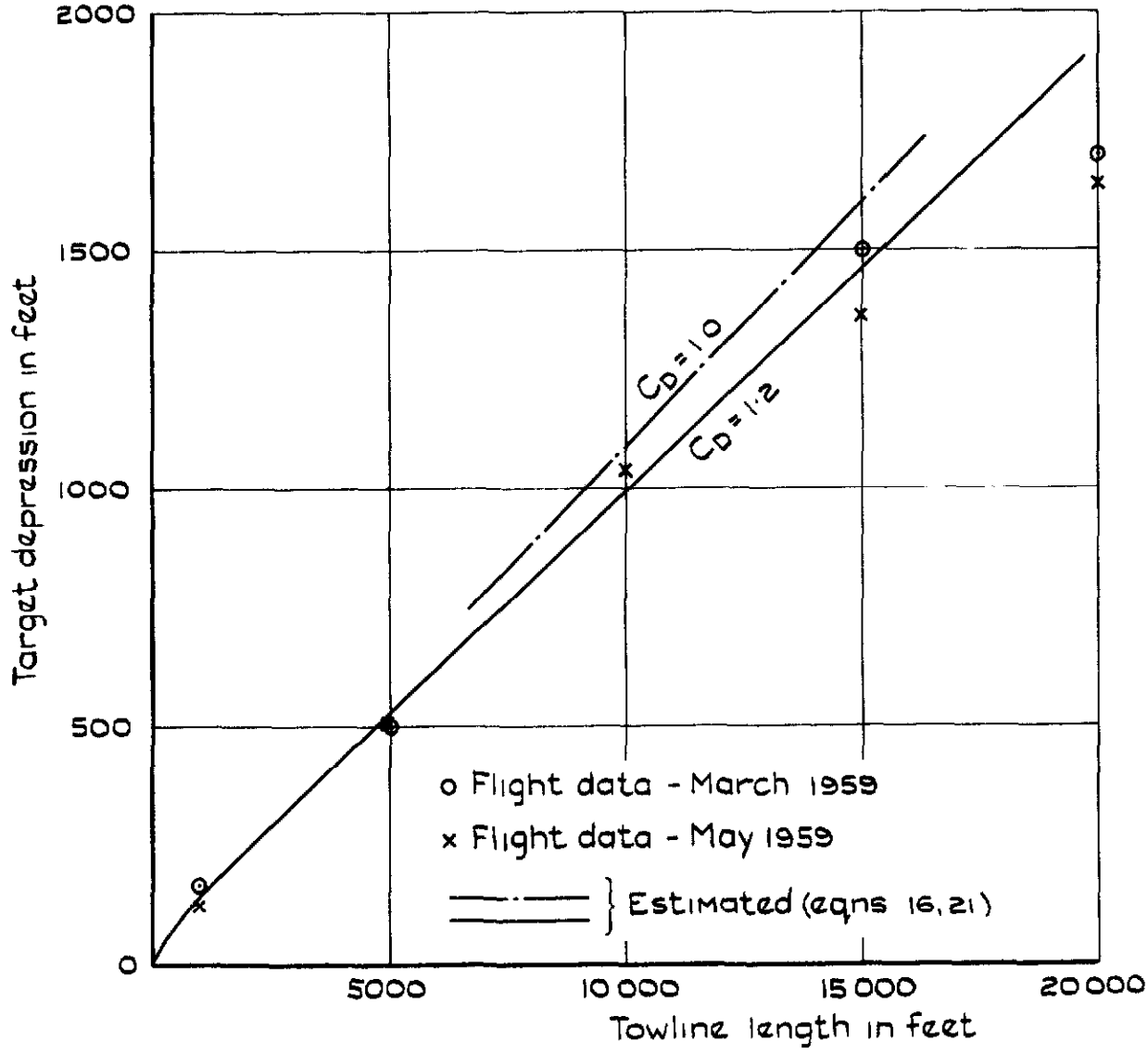

c ias 200kt

Fig. 20 contd

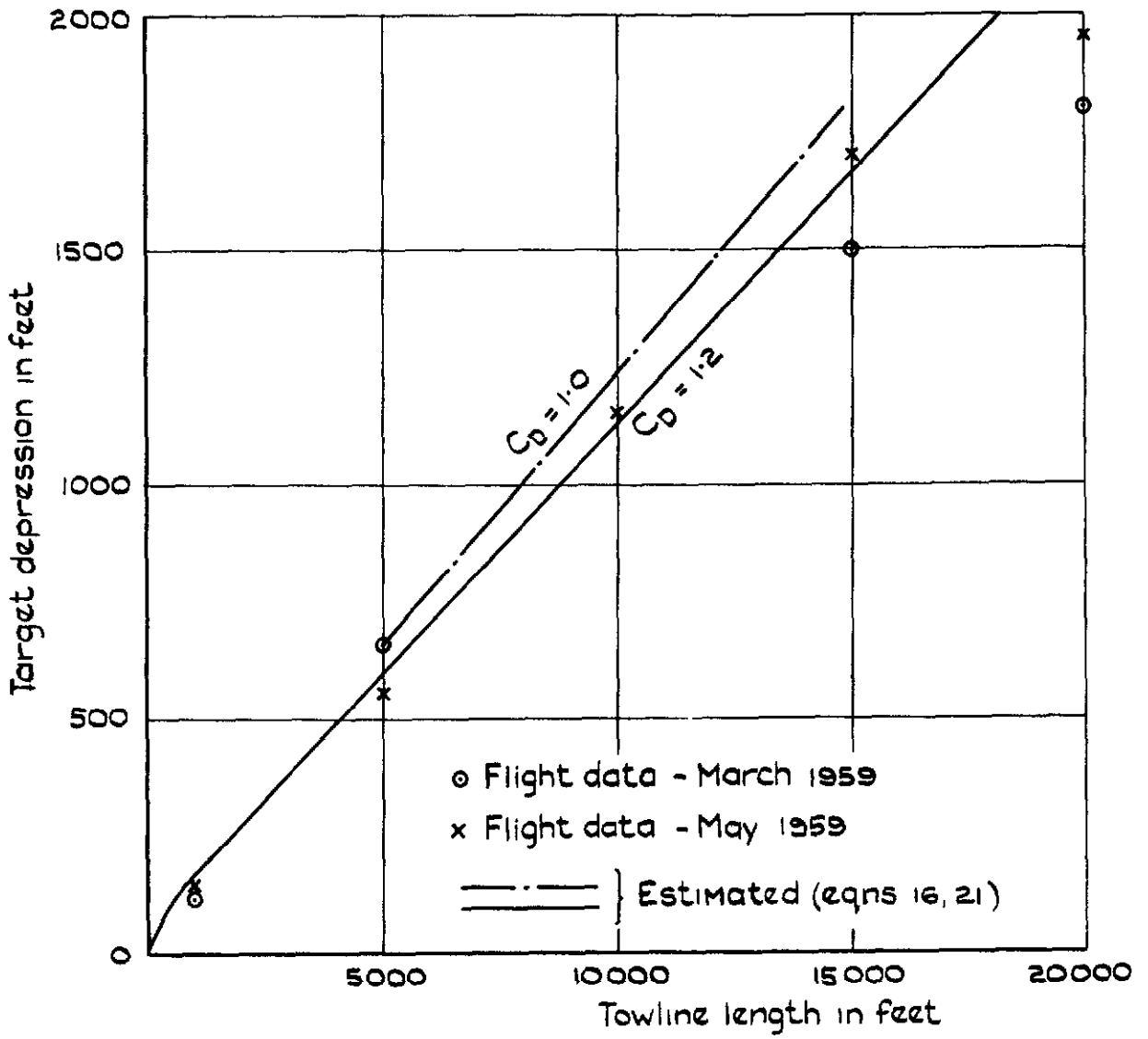

d ias 175 kt

Fig. 20 concld

Printed in England for Her Majesty's Stationery Office by the
Royal Aircraft Establishment, Farnborough Dd 503427 K4 11/72

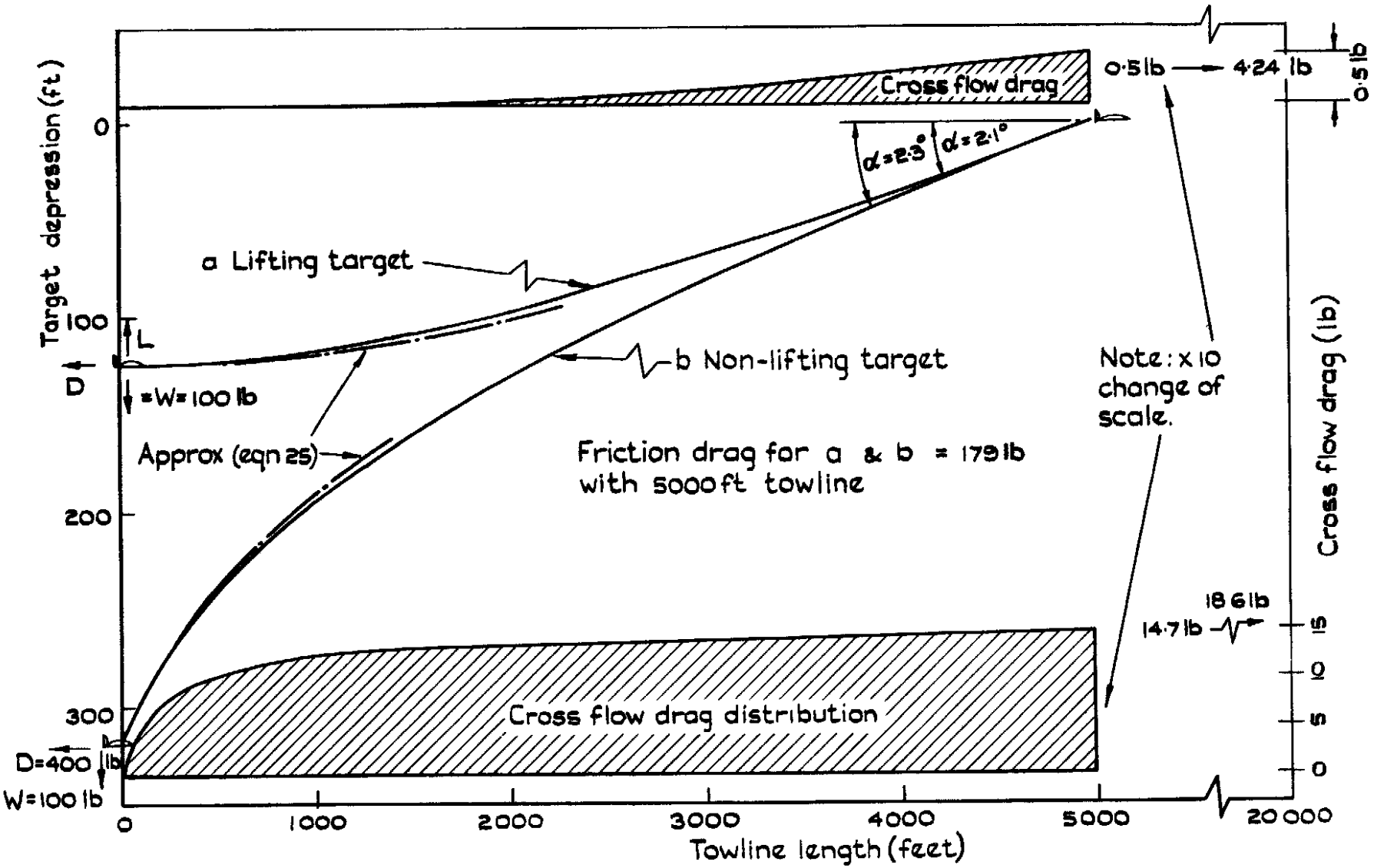

Fig. 21 Line shape and cross flow drag distribution for a particular lifting & non-lifting supersonic target. (M = 1·6, 40 000 ft altitude)

ARC CP No 1235
July 1968

D Pierce and
L J Beecham

SOME AERODYNAMIC CONSIDERATIONS OF THE FLIGHT CHARACTERISTICS OF TOWING SYSTEMS USING LONG TOWLINES AT HIGH SPEEDS

This Paper describes wind-tunnel experiments at supersonic speeds on the characteristics of the three-dimensional growth of turbulent boundary layers on long axi-symmetrically placed wires

The results have led to the development of a method of calculating the tension and drag distribution along, and the shape of, long towlines as used in aircraft target towing systems

ARC CP No 1235
July 1968

D Pierce and
L J Beecham

SOME AERODYNAMIC CONSIDERATIONS OF THE FLIGHT CHARACTERISTICS OF TOWING SYSTEMS USING LONG TOWLINES AT HIGH SPEEDS

This Paper describes wind-tunnel experiments at supersonic speeds on the characteristics of the three-dimensional growth of turbulent boundary layers on long axi-symmetrically placed wires

The results have led to the development of a method of calculating the tension and drag distribution along, and the shape of, long towlines as used in aircraft target towing systems

DETACHABLE ABSTRACT CARDS

ARC CP No 1235
July 1968

D Pierce and
L J Beecham

SOME AERODYNAMIC CONSIDERATIONS OF THE FLIGHT CHARACTERISTICS OF TOWING SYSTEMS USING LONG TOWLINES AT HIGH SPEEDS

This Paper describes wind-tunnel experiments at supersonic speeds on the characteristics of the three-dimensional growth of turbulent boundary layers on long axi-symmetrically placed wires

The results have led to the development of a method of calculating the tension and drag distribution along, and the shape of, long towlines as used in aircraft target towing systems

DETACHABLE ABSTRACT CARDS

Cut here

Cut here

These abstract cards are inserted in Technical Reports for the convenience of Librarians and others who need to maintain an Information Index

Published by
HER MAJESTY'S STATIONERY OFFICE

To be purchased from
49 High Holborn, London WC1 V 6HB
13a Castle Street, Edinburgh EH2 3AR
109 St Mary Street, Cardiff CF1 1JW
Brazennose Street, Manchester M60 8AS
50 Fairfax Street, Bristol BS1 3DE
258 Broad Street, Birmingham B1 2HE
80 Chichester Street, Belfast BT1 4JY
or through booksellers

C.P. No. 1235

SBN 11 470793 6